Response of the sea-ice diatom Fragilariopsis cylindrus to simulated polar night darkness and return to light

Philippe-israël Morin, Thomas Lacour, Pierre-luc Grondin, Flavienne Bruyant, Joannie Ferland, Marie-hélène Forget, Philippe Massicotte, Natalie Donaher, Douglas A Campbell, Johann Lavaud, et al.

Response of the sea-ice diatom *Fragilariopsis cylindrus* to simulated polar night darkness and return to light

Morin, Philippe-Israël[1]; Lacour, Thomas[2]; Grondin, Pierre-Luc[1]; Bruyant, Flavienne[1]; Ferland, Joannie[1]; Forget, Marie-Hélène[1]; Massicotte, Philippe[1]; Donaher, Natalie[3]; Campbell, Douglas A[3]; Lavaud Johann[1] & Babin, Marcel[1]

[1]UMI 3376 Takuvik, CNRS/Université Laval, Département de Biologie-Pavillon Alexandre Vachon, Québec, QC, G1V 0A6, Canada

philippe-israel.morin.1@ulaval.ca

pierre-luc.grondin.1@ulaval.ca

flavienne.bruyant@takuvik.ulaval.ca

Joannie.Ferland@takuvik.ulaval.ca

Marie-Helene.Forget@takuvik.ulaval.ca

philippe.massicotte@takuvik.ulaval.ca

Johann.Lavaud@bio.ulaval.ca

Marcel.Babin@takuvik.ulaval.ca

[2]Ifremer, PBA, Rue de l'Ile d'Yeu, BP21105, 44311 Nantes Cedex 03, France

Thomas.Lacour@ifremer.fr

[3]Mount Allison University, Sackville, NB, E4L 3M7, Canada

dcampbell@mta.ca

ndonaher@mta.ca

Author for correspondence:

Philippe-Israël Morin

Tel: +1 418 656 5193

Email: philippe-israel.morin.1@ulaval.ca

Running head: Diatoms polar night darkness survival

Abstract

Arctic photoautotrophic communities must survive through polar night darkness until light returns in spring. We tracked changes in the cellular resource allocations and functional capacities of a polar sea-ice diatom, *Fragilariopsis cylindrus*, to understand acclimation processes in both darkness and during the subsequent return to light. We measured parameters at specific time-points over 3 months of darkness, and then over 6 days after a return to light. Measured parameters included cell number and size, cellular carbon and nitrogen quotas, lipid and pigment contents, concentration of key proteins of the photosynthetic system, photosynthetic parameters based on both variable fluorescence and carbon assimilation, and the level of non-photochemical quenching.

A stable functional state was reached within a few days after the transition to dark and was then maintained throughout three months of darkness. The dark period resulted in a decrease of lipid droplet cell quota (-6%), chlorophyll *a* cell quota (-41%) and the maximum carbon fixation rate per cell (-98%). Return to light after 1.5 months of darkness resulted in a strong induction of non-photochemical quenching of excitation and a fast recovery of the maximum carbon fixation rate within 1 day, followed by a rapid increase in the cell number. Return to light after three months of darkness showed an increase of mortality or a profound down-regulation induced over longer periods of darkness.

Keywords: *Fragilariopsis cylindrus*, sea-ice diatom, diatoms, acclimation, dark survival, polar night, light return, darkness

Introduction

Diatoms experience a wide range of environmental conditions across the oceans, with some imposing extreme stresses upon the cells. Light spans one of the largest ranges of environmental variation as diatoms may transition from high light exposure in the sunlit surface layer to darkness due to ocean mixing or during the night. Beyond diel cycles, diatoms may survive weeks in total darkness during deep ocean mixing events (Cullen & Lewis 1988; Marshall & Schott 1999), and possibly up to centuries during sedimentation events (McQuoid et al. 2002; Godhe & Härnström 2010; Härnström et al. 2011). At high latitudes, darkness sometimes lasts as long as ca. six months as a consequence of the sea ice covered with snow and low or even negative sun elevation during the polar night. Given the photoautotrophic nature of diatoms, their survival of a lack of sunlight for up to 6 months is remarkable and has motivated many studies in the past decades to understand the related acclimation processes.

So far, in experiments studying the response to prolonged darkness, microalgal or diatom cell growth recovered after the imposed dark period (Table 1). Spore production might explain diatom survival during prolonged darkness (Doucette & Fryxell 1983), but spores have only rarely been observed in experiments (Peters & Thomas 1996; Zhang et al. 1998). A "vegetative" or physiological resting state could be more prevalent for overwintering as resting cells have the ability to rapidly recover to their active state (Anderson 1975; Sicko-Goad et al. 1986). Heterotrophic nutrition has also been considered as a means for dark survival (Lewin 1953; White 1974; Hellebust & Lewin 1977), but the extent of its contribution remains uncertain, as it is not always detected (Horner & Alexander 1972; Popels et al. 2002; McMinn & Martin 2013).

In several experiments on microalgae, not all on polar diatoms, a physiological resting state during prolonged darkness has been characterized by a low rate of metabolic activities. The metabolic activity of chlorophytes was greatly lowered after 10 days in the dark (Jochem 1999). The particulate organic carbon and nitrogen cell quotas in three Antarctic diatoms remained stable over 80 days in the dark, also suggesting a lowered metabolism with

limited consumption of reserves (Peters & Thomas 1996). Despite low rates of metabolic activity, consumption of energy reserves likely fuels basal metabolic needs shortly after transition to total darkness (Palmisano & Sullivan 1982). Mock et al. (2017) found that 60% of all genes were down-regulated in the *F. cylindrus* transcriptome after 7 days of darkness, but genes involved in starch, sucrose and lipid metabolism were up-regulated. Schaub et al. (2017) also found patterns of lipid consumption in a benthic Arctic diatom to be faster in the first two weeks of a two-month long dark experiment. In other experiments with either a temperate diatom (Handa 1969), a *Chlorophyceae* (Dehning & Tilzer 1989) or a *Pelagophyceae* (Popels et al. 2007), similar patterns of rapid consumption early during the dark period occurred with preferential catabolism of proteins and carbohydrate reserves.

Photophysiology also appears to be strongly downregulated in prolonged darkness. Among *Chlorophycaeae* (Hellebust & Terborgh 1967; Dehning & Tilzer 1989), *Pelagophyceae* (Popels et al. 2007) and temperate (Griffiths 1973) or polar (Peters & Thomas 1996) diatoms, the maximum rate of carbon fixation (P_{max}) per chlorophyll *a* (Hellebust & Terborgh 1967; Griffiths 1973; Dehning & Tilzer 1989; Popels et al. 2007) or per cell (Peters & Thomas 1996) strongly decreased within the first weeks under prolonged darkness. In the experiment of Popels et al. (2007), a drop in the absolute concentration of carbon fixation enzyme RuBisCO was also detected. Lacour et al. (2019), however, recently measured in a polar diatom a rather stable level of RuBisCO-to-carbon ratio, despite a strong decrease in P_{max} per carbon in prolonged darkness. In other studies, the maximum quantum yield of photochemistry (Φ_M) and the maximum relative electron transport rate (rETRmax) also decreased within several weeks of darkness whether studying polar algal communities (Martin et al. 2012), cultures of polar diatoms (Reeves et al. 2011; Lacour et al. 2019), benthic diatom communities (Wulff et al. 2008) or even *Rhodophyta* thalli (Luder et al. 2002).

At the structural level of the photosynthetic apparatus, the molecular components of the light-harvesting antennae (pigments, proteins) of a green algae (Baldisserotto *et al.,* 2005a; Ferroni *et al.,* 2007) and a *Xanthophyceae* (Baldisserotto *et al.,* 2005b) were partially

dismantled or degraded after 2-3 months of darkness. However, in these experiments, the light-harvesting antennae appeared to keep a certain level of organization to re-use light as soon as it became available once again. Generally, a decrease in the chlorophyll *a* cell quota or absolute concentration occurred in previous dark experiments (Table 1), though not always, particularly for dark experiments shorter than 1 month. Chlorophyll *a* remained stable in these shorter term experiments whether expressed as cell quota (Hellebust & Terborgh 1967; Doucette & Fryxell 1983), absolute concentration (Griffiths 1973; Popels et al. 2007; Reeves et al. 2011) or chl-to-carbon ratio (Lacour et al. 2019). In benthic diatoms, Veuger & van Oevelen (2011) also measured a decrease in the dry weight concentration of other pigments, including the photoprotective diadinoxanthin/diatoxanthin pigments, with the largest decrease attributable to the photosynthetic ones (chloroyphyll *a,* chloroyphyll *c,* Fucoxanthin).

In polar regions, when the polar night ends, incident irradiance increases, the snow and sea-ice covers then melt, and spring blooms of ice algae and phytoplankton take place (Wassmann & Reigstad 2011). Much of the annual production, and most of the new production in the Arctic Ocean, occur at that time of the year (Sakshaug 2004; Perrette et al. 2011; Ardyna et al. 2013). Sea-ice algae dominated by pennate diatoms are the first to exploit the return of light in spring, before the phytoplankton bloom develops (Mundy et al. 2005; Leu et al. 2015; Wassmann 2011). At least a few diatom cells from all species present at any time in polar oceans must survive overwintering in the full darkness to inoculate the populations that grow during summer. The stress imposed by the return of light in spring may further compromise the survival of overwintering populations after such a long period of darkness. Thus, their ability to recover is of crucial importance as regard to their fate.

Despite the numerous studies on microalgae dark survival, only a few have measured physiological parameters during the recovery upon light return (Table 1). In general, the low photosynthetic performances observed during the dark period, whether measured at the photochemistry level (Luder et al. 2002; Wulff et al. 2008; Martin et al. 2012), the carbon

144 fixation level (Griffiths 1973; Peters & Thomas 1996; Popels et al. 2007) or both (Kvernvik
145 et al. 2018; Lacour et al. 2019), recover within the first days of re-illumination. Peters &
146 Thomas (1996) and Popels et al. (2007) also measured a recovery in particulate nitrogen
147 and carbon levels which requires energy to be available rapidly after re-illumation. Recent
148 studies on polar phytoplankton communities (Kvernvik et al. 2018) and a polar diatom
149 culture (Lacour et al. 2019) focused on the ability to restore growth with different
150 irradiance intensities. Regardless of the light intensity, polar microalgae appeared to
151 recover their photophysiological capacity within 48 hours.
152
153 Although dark survival of microalgae has received considerable attention in the past
154 decades, our understanding of more specifically polar night darkness survival in diatoms
155 remains limited for several reasons. Some of the former studies have shown dark survival
156 for numerous microalgal species over periods representative of the polar night and even
157 beyond (rows 3,5,9,10,13-15,18-20,23,26-28, Table 1). They however documented a
158 limited suite of physiological and biochemical parameters, which did not allow to fully
159 understand the involved cellular mechanisms. Some other experiments did measure several
160 parameters and provided a complete transcriptional profiling of sequenced genes, but for
161 only a short dark period (< 20 days) (rows 4,6, Table 1); 3) Other experiments studied non-
162 polar species (or not diatoms) with detailed characterization and are to be interpreted with
163 caution relative to diatoms in the polar environment (rows 12,21, Table 1); 4). A
164 combination of these limitations is not uncommon (rows 7,8,11,16,17,22,24,25,29-31,
165 Table 1).
166 Our study (row 1, Table 1) aimed at overcoming the limitations described above with an
167 integrative characterization of a sea ice diatom, *Fragilariopsis cylindrus*, tracking
168 physiological and metabolic acclimation over a darkness period representative of the polar
169 night, and over its resumption of growth upon return to light. Our results are largely
170 consistent with earlier findings on parameters measured in common across the studies, but
171 we significantly expand previous knowledge by parallel monitoring of multiple
172 physiological and metabolic features.
173

Table 1 Chronological list of dark survival experiments for microalgal species with the present study highlighted.

	Species	Length of experiment (days)	Parameters				T(°C)	References
			Cell	Metabolism and Reserves	Photosynthetic apparatus			
					Molecular components	Photophysiology		
1	*Fragilariopsis cylindrus*	D: 90 L: 6*	Number Volume	POC & PON Lipids	Pigments RbcL, PsbA	^{14}C P. vs E. curves Fluo	0	This study
2	*Chaetoceros neogracile*	D: 30 L: 8,14	Number Volume	POC & PON	Pigments RbcL	^{14}C P. vs E. curves Fluo	0	Lacour *et al.*, 2019
3	Arctic phytoplankton community of polar night	D: *in situ* L: 2	N/A	N/A	Chl*a*	^{14}C uptake Fluo	1.5, 2	Kvernvik *et al.*, 2018
4	*Fragilariopsis cylindrus*	D: 7	N/A	Gene expression	Gene expression	N/A	-2, 11	Mock *et al.*, 2017
5	*Navicula cf. perminuta*	D: 56	N/A	Lipids, Prots, Carbs	N/A	N/A	0, 7	Schaub *et al.*, 2017
6	*Phaeodactylum tricornutum*	D: 2 L: 1	Number Morphology	N/A	Pigments Gene expression	Fluo	15	Nymark *et al.*, 2013
7	Polar algal communities	D: 22-35 L: 1	N/A	Carbs	Chl*a*	Fluo	-2, 4, 10, 20	Martin *et al.*, 2012
8	*Fragilariopsis cylindrus* *Thalassiosira antartica…*	D: 30-60 L:growth**	N/A	Carbs	Chl*a*	Fluo	-2, 4, 10	Reeves *et al.*, 2011
9	Diatom sediment samples	D: 371 L: 1	N/A	N/A	Pigment content (Dark only)	^{13}C uptake (Light only)	17	Veuger & Van Oevelen 2011
10	Sediment sample / isolation of *Skeletonema marinoi*	D: >100 y L: N/A	Growth (Light only)	N/A	N/A	N/A	10	Harnstrom *et al.*, 2011
11	Diatom sediment samples	D: 15-64 L: 1-4 h	N/A	N/A	N/A	Fluo	4-6	Wulff *et al.*, 2008
12	*Aureococcus anophagefferens*	D: 14 L: 4-5*	Number Bacteries	POC & PON, Lipids, Prots, Carbs	Chlorophyll *a* RbcL	^{14}C P. vs E. curves Fluo	6	Popels *et al.*, 2007
13	*Koliella antartica*	D:60	Morphology	N/A	Chl*a,b* PSII assembly	N/A	5	Ferroni *et al.*, 2007
14	*Xanthonema* sp. *Koliella antartica*	D: 60-90	Number Morphology	N/A	Chl*a,b*,carotenoid PSII assembly	N/A	4, 5	Baldisserotto *et al.*, 2005
15	Diatom sediment samples	D: > 55 y L: 30-40	Growth (Light only)	N/A	N/A	N/A	3, 10, 18	McQuoid *et al.*, 2002
16	*Palmaria decipiens*	D: 180 L: 28	N/A	N/A	N/A	Fluo	0	Luder *et al.*, 2002

17	*Brachiomonas submarina* *Pavlova lutheri…*	D: 10-12 L: 5	Number	Metabolic activity Heterotrophy	N/A	N/A	10	Jochem 1999
18	Polar algal communities	D: 161 L: 30	Number	N/A	N/A	N/A	1	Zhang 1998
19	*Thalassiosira antartica* *Thalassiosira tumida …*	D: 72-302 L: 5-30*	Number	POC & PON	Chl*a*	^{14}C uptake	0	Peters & Thomas 1996
20	*Thalassiosira punctigera* *Rhizosolenia setigera…*	D: 30-70 L: 8-20*	Number	POC & PON	Chl*a*	^{14}C uptake	8, 15	Peters 1996
21	*Scenedesmus acuminatus*	D: 90 L: growth**	Number Volume	Lipids, Prots, Carbs, Dry weight, Heterotrophy	Chl*a* Phaeopigments	^{14}C P. vs E. curves	7, 22	Dehning & Tilzer 1989
22	*Thalassiosira antartica* var. arctica	D: 10	Number Spores	POC & PON	Chl*a*	N/A	4	Doucette & Fryxell 1983
23	*Nitzschia cylindrus* Araphid pennate diatom specie	L-D: 30 D: 150	Number Morphology	N/A	N/A	N/A	0,-2	Palmisano & Sullivan 1983
24	*Nitzschia cylindrus* Araphid pennate diatom specie	L-D: 30	Number	Respiration, Heterotrophy Lipids, Prots, Carbs, ATP	N/A	^{14}C uptake	0,-2	Palmisano & Sullivan 1982
25	*Nitzschia angularis var.Affinis* *Cyclotella cryptica…*	D:10-20	N/A	Heterotrophy	N/A	N/A	20	Hellebust & Lewin 1977
26	*Thalassiosira pseudonana* *Phaeodactylum tricornutum…*	D: < 365 L: < 64	Number	N/A	N/A	N/A	2,10, 20	Antia 1976
27	*Cyclotella cryptica* *Coscinodicus sp.*	D: 1 year L: growth**	Number Volume	POC & PON Heterotrophy	Chl*a* ,c	^{14}C uptake	18,20	White 1974
28	*Thalassiosira gravida* *Ditylum brightwellii…*	D: 90 L: growth**	Number	N/A	N/A	N/A	15	Smayda & Mitchell 1974
29	*Phaeodactylum tricornutum*	D: 7-16 L: 7	Number	Prots	Chl*a*	^{14}C uptake	18,28	Griffiths 1973
30	*Skeletonema costatum*	D:10	N/A	POC & PON, Lipids, Prots, Carbs	Chl*a*	^{14}C uptake	18	Handa 1969
31	*Dunaliella tertiolecta*	D: 7	Number	POC	Chl*a*	^{14}C P. vs E. curves RuDP activities	18	Hellebust & Terborgh 1967

The length of each experiment is shown in days, hours-h or years-y when specified for Dark (D) and Light (L) return experiments. The measured parameters are separated into four categories (Cell, Metabolism, Molecular components and Photophysiology of the Photosynthetic apparatus). T is the temperature in Celsius degrees. Abbreviations: L = Light return, D =Dark, L-D= Light-Dark transition, POC & PON = Particular Organic Carbon & Nitrogen, Prots = Proteins, Carbs = Carbohydrate, ATP = Adenosine triphosphate, ^{14}C & ^{13}C = Radiocarbon, ^{14}C P. vs E. curves = Photosynthesis versus Irradiance curves of ^{14}Carbon fixation, Fluo = Fluorescence determinations (PSII variable fluorescence and/or spectrofluorimetry), Chl*a-b-c* = Chlorophyll *a-b-c,* PSII = Photosystem II, PsbA = PSII protein D1, RbcL = RuBisCO large subunit.

* indicates two or more light return experiments.

** indicates only growth potential was verified upon a light return.

… indicates more species were studied.

Materials & Methods

Cell culturing

Axenic cultures of *Fragilariopsis cylindrus* (Grunow) Krieger (strain NCMA3323) were freshly obtained from the National Center for Marine Algae and Microbiota. *F. cylindrus* is the only polar diatom with a sequenced and published genome (see Mock et al. 2017). It was grown in semi-continuous cultures in pre-filtered L1 medium (Guillard & Hargraves 1993). Cultures in triplicate were started in 50 ml borosilicate tubes and then sequentially transferred to larger vessels several times until a final transfer of 5 l of culture to 20-l polycarbonate round vessels (Fig. S1). Thereafter, further additions of L1 media served to increase culture volume while matching growth rate so that the cell density remained steady (Wood et al. 2005). Light was provided continuously with DURIS® E3 LED bands (GW JCLMS1.EC, 4000 K) at a scalar irradiance of approximately 30 μmol photons m^{-2} s^{-1} as measured with a QSL-100 quantum sensor (Biospherical instruments, San Diego, CA, USA) placed in the centre of the vessel. Scalar irradiance ranged from 29.5 to 33.5 μmol photons m^{-2} s^{-1} depending on the culture vessel position in the growth chamber (Fig. S1). This irradiance was chosen based on the irradiance at which the growth rate saturated (K_E): 0.244±0.041 d^{-1}. Each culture was gently mixed with a 12.5 cm magnetic stirrer and bubbled with air filtered through a 0.3 μm capsule filter (Carbon CAP, Whatman™ 6704-7500). Temperature of the growth chamber (CARON, model 7901-33-2) was kept at 0°C for the duration of the experiment.

Sampling design

The first two samplings took place once the growth rate, cell diameter and Chlorophyll *a* (Chl*a*) were steady for a minimum of 10 cell generations (MacIntyre & Cullen 2005a), one day before the transition from light to dark (referred to as the -1-day sampling), and on the day of the transition just before turning off the light (referred to as the 0-day sampling). Both are collectively referred to as light-acclimation sampling days. In order to avoid light limitation of growth, the cultures were kept optically thin during the acclimation period (between 4×10^4 to 6×10^5 cell mL^{-1}). The cell suspension density was ~ 5×10^5 cell ml^{-1}

before the dark transition. The light system was then switched off and each vessel was carefully covered with opaque material. Sampling in the dark began 24 hours following the transition and subsequent dark samplings followed after 5, 14, 28, 63 and 83 days of darkness as shown with the timeline in Fig. 1. Syringes used for sampling culture volume were completely opaque, as well as the tubes connecting to the cultures vessels, and all sub-samples were contained in opaque tubes until their respective measurements. Every immediate manipulation (e.g. filtrations, fluorescence determinations and ^{14}C incubations) was completed under very low green light levels in order to avoid excitation of the photosystems. The Light return 1 experiment took place after 1.5 months (48 days) of darkness. Culture volume was carefully transferred to gently aerated 3-l vessels cooled to 0°C and illuminated at 30 μmol photons m^{-2} s^{-1} with a slightly different light spectrum (Fig. S2). This second light system was provided by a customized LED system comprising 8 colours independently variable in intensity and mounted on 6 LED panels around the 3-l vessels (Fig. S3). The cultures were sampled at 30 minutes, 2 hours, 5 hours, 1 day, 3 days and 6 days following re-illumination (Fig. 1). The Light return 2 experiment took place after 3 months (90 days) in the dark following the same procedure (Fig. 1). All manipulations were completed under very low green light levels for both light return experiments (See background light in Fig. S3)

At sampling time-points culture samples were harvested to measure the parameters described below with a few exceptions. The relative electron transport rate (rETR) and non-photochemical quenching (NPQ) were measured for the light return experiments and for several time-points during the dark period (14, 28, 47 and 83 days). Carbon fixation rates were measured at all points except after 3 months of darkness. Lipid droplets were measured from 5 hours to 6 days following both light return experiments and for every time-point during the dark period. The maximum quantum yield of PSII (Photosystem II) photochemistry (Φ_M) and the effective absorption cross-section (σ_{PSII}) were also measured 2 days after the transition to dark. Table 1 summarizes the measurements made for every sampling time-point.

Table 2 : Sampling time-points of the parameters measured during the dark and light experiments

Time	[1]Cell number & volume	[2]Carbon & nitrogen	[3]Lipid droplets	[4]Pigment	[5]Photosynthetic proteins	[6]Variable fluorescence (FIRe)	[7]Variable fluorescence (PAM)	[8]incubations (^{14}C)
D : -1 day	X	X	X	X	X	X		X
D : 0 days	X	X	X	X	X	X		X
D : 1 day	X	X	X	X	X	X		X
D : 2 days						X		
D : 5 days	X	X	X	X	X	X		X
D : 14 days	X	X	X	X	X	X	X	X
D : 28 days	X	X	X	X	X	X	X	X
D : 47 days							X	
D : 63 days	X	X	X	X	X	X		
D : 83 days	X	X	X	X	X	X	X	X
L1 : 30 min	X	X		X	X	X	X	X
L1 : 2 hours	X	X		X	X	X	X	X
L1 : 5 hours	X	X	X	X	X	X	X	X
L1 : 1 day	X	X	X	X	X	X	X	X
L1 : 3 days	X	X	X	X	X	X	X	X
L1 : 6 days	X	X	X	X	X	X	X	X
L2 : 30 min	X	X		X	X	X	X	X
L2 : 2 hours	X	X		X	X	X	X	X
L2 : 5 hours	X	X	X	X	X	X	X	X
L2 : 1 day	X	X	X	X	X	X	X	X
L2 : 3 days	X	X	X	X	X	X	X	X
L2 : 6 days	X	X	X	X	X	X	X	X

D=Dark experiment, L1 = Light return 1 experiment, L2 = Light return 2 experiment, **1:** Cell number per mL and cell volume (μm^3), **2:** Carbon & Nitrogen cell quotas, **3:** Lipid droplets cell quota, **4:** Pigment (Chlorophyll *a*, Chlorophyll *c*, Fucoxantin, Diadinoxanthin, Diatoxanthin) cell quotas, **5:** PsbA (PSII protein D1) & RbcL (RuBisCO large subunit) cell quotas, **6:** Maximum quantum yield (Φ_M) and the effective absorption cross-section for PSII photochemistry (σ_{PSII}), **7:** Relative electron transport rate (rETR) and non-photochemical quenching (NPQ), **8:** Carbon fixation rate ($\mu g\ C\ m^{-3}\ h^{-1}$)

Cell number and volume and culture axenicity

Cells were counted and sized using a Beckman Multisizer 4 Coulter Counter. Three consecutive countings were recorded for each culture sampling point. Total cell counts did not differentiate cell viability; hence mortality could not be assessed through this method. However, mortality can be suspected when looking at the flow cytometry data (see Lipid droplets section and Fig. S4). The flow cytometry data indicated that the number of debris, likely the result of dying cells, appeared to increase with the duration of the experiment, especially during the Light return 2 experiment. The cell volume was calculated using the sphere-equivalent diameter. The biovolume was calculated as cell volume x cell number for each culture. Axenicity of each culture was verified with petri dishes prepared as described in MacIntyre & Cullen (2005b). Axenicity was confirmed once before the acclimation period.

Carbon and nitrogen cell content

Three technical replicates were harvested per algal culture; aliquots of 20 ml were filtered onto binder-free glass-fiber filters (GF/F) (0.7 µm, 25 mm) pre-combusted at 500°C for 24 hours. Filters were then dried at 60°C for at least 12 hours and kept desiccated before elemental analysis with a CHN analyzer (2400 Series II CHNS⁄O; Perkin Elmer, Norwalk, CT, USA).

Lipid droplets

Cells were assessed for their lipid droplets content using the molecular probe BODIPY® 505/515 (www.lifetechnologies.com) according to Brennan et al. (2012) using a flow cytometer (488 nm excitation, 520 nm emission, Millipore Guava easycyte flow cytometer) in a 96-well plate. BODIPY fluorescence emitted from the lipid droplets was quantified for each cell as relative fluorescence units (RFU). For samples analyzed at each time-point, a total of 9 wells were prepared (three technical replicates per culture) and BODIPY fluorescence was measured on 5000 cells for each well. Before fluorescence measurements, samples were incubated for 1 h on ice in the dark. Each well contained 300 µl of algal culture marked with 4 µl of a BODIPY solution (final concentration 0.33 µM / 1.32%

DMSO). For each time-point sampling, technical replicates were pooled together for each culture and averaged for their mean RFU according to a target function (Fig. S4).

Pigment content

For each culture, 10 ml were filtered onto glass-fiber filters (GF/F) (0.7 μm, 25 mm, Millipore). Filters were immediately flash-frozen in liquid nitrogen and stored at -80°C until analysis. Pigment separation was performed with high performance liquid chromatography (HPLC) according to Zapata et al. (2000). Before HPLC analyses, pigments were extracted in 95% methanol and sonicated for 20 seconds three times. Samples were then centrifuged (4500 rpm) 15 minutes at 4°C and filtered on polytetrafluoroethylene (PTFE) membranes (0.2 μm). Data were analysed using the ChromQuest 5.0 software.

Photosynthetic proteins

For PsbA (PSII protein D1) and RbcL (RuBisCO large subunit) quantification, 30 ml of each culture was harvested onto GF/F filters, flash-frozen and stored at -80°C. Protein extraction was performed using the FastPrep-24 and bead lysing 'matrix D' (MP Biomedicals), using 3 cycles of 60 seconds at 6.5 m s^{-1} in 300 μL of 1X extraction buffer (Agrisera AS08_300 with 0.4 M of the protease inhibitor AEBSF added), then spun at 16 000 g for 5 minutes (Li & Campbell, 2013). For each protein extract supernatant we then estimated the content of total nitrogen derived from the original sample using the parallel determinations of total N content per mL of sample. We then loaded each well of gels with a volume of protein extract sufficient to deliver equivalent total nitrogen across wells. We chose this approach for loading because total nitrogen determinations are more reliable than total protein determinations. Separation of proteins was done in a Bolt 4-12% Bis Tris SDS-PAGE gel (Invitrogen). Proteins were quantified by western-blotting with anti-PsbA (AS05 084) or anti-RbcL (AS01 017) antibodies (www.agrisera.se) (Li et al. 2016). Chemiluminescent images were obtained using ECL Ultra reagent (Lumigen, TMA-100) and a VersaDoc CCD imager (Bio-Rad). Band densities for samples were determined against the standard curve using the ImageLab software (v 4.0, Bio-Rad).

Variable fluorescence

Variable in vivo Chl*a* fluorescence at 680 nm was measured using a Fluorescence Induction and Relaxation (FIRe) fluorometer (Satlantic, Halifax, NS, Canada) that applies a saturating, single turnover flash (STF, 100 μs) of blue light (455 nm, 60-nm bandwidth) to the sample. Based on the fluorescence induction curve, the FIReWORX algorithm (Audrey Barnett, www.sourceforge.net) estimates the effective absorption cross-section for PSII photochemistry (σ_{PSII}, Å^2 quanta^{-1}), the minimum flux of fluorescence (F_0) and the maximum flux of fluorescence of dark acclimated cells (F_m) in relative units (Kolber et al. 1998). σ_{PSII}, F_0 and F_m were measured on culture sub-samples shortly after harvesting along the dark acclimation and during the Light return 1 and Light return 2 experiments, after 30 minutes of dark acclimation. The maximum quantum yield of PSII (Φ_M) was computed as:

$$\Phi_M = \frac{F_v}{F_m} = \frac{F_m - F_0}{F_m} \quad (1)$$

A Phyto-PAM fluorometer (Phyto-ML, Heinz Walz GmbH, Germany) was also used to assess complementary fluorescence parameters. Using a different fluorometer did not compromise the interpretation of the data altogether, as the trends in Φ_M were similar for both FIRe and Phyto-PAM determinations (Fig S5). Phyto-PAM determinations are typically higher than FIRe determinations, but their relative variations are equivalent and comparable (Röttgers 2007). For the Phyto-PAM fluorometer, cells were dark-acclimated for 30 minutes when applicable (Light return 1 and Light return 2 experiments) and subsequently exposed to a rapid light curve (RLC) protocol using 8 step-wise increasing irradiances from 1 to 111 μmol photons m^{-2} s^{-1} and for 10 or 30 seconds each (Lefebvre et al. 2011). After each irradiance-step, F_m' was probed with an actinic flash (500 ms), while a detecting modulated light source measured F_s. Although the instrument allows excitation of fluorescence at four different wavelengths, actinic light was only provided by the actinic LEDs peaking at 655 nm (Fig. S2). To calculate the PSII-specific rETR, the achieved quantum yield of charge separation in PSII (Φ_{PSII}) at each irradiance step was multiplied by the corresponding irradiance (E):

$$\Phi_{PSII} = \frac{F_m' - F_s}{F_m'} \quad (2a)$$

$$rETR = \Phi_{PSII} \cdot E \quad (2b)$$

where F_m' and F_s are the maximum and steady-state fluorescence of light acclimated cells, respectively. To calculate the maximum relative electron transport rate (rETRmax), a function was fitted to the data by least-square fit according to Eilers & Peeters (1988):

$$rETR(E) = \frac{E}{aE^2+bE+c} \quad (3)$$

where a, b and c are expressed as:

$$a = \frac{1}{s \cdot I_m} \quad (4a)$$

$$b = \frac{1}{P_m} - \frac{2}{s \cdot I_m} \quad (4b)$$

$$c = \frac{1}{s} \quad (4c)$$

and where s is the initial slope, I_m is the optimal irradiance and P_m is the maximal production rate of the fit. The dynamic non-photochemical quenching (NPQd, also referred as NPQ in the text) was calculated for each irradiance-step as:

$$NPQd = \frac{F_m - F_m'}{F_m'} \quad (5)$$

and the sustained and total non-photochemical quenching (NPQs, NPQt) were calculated as:

$$NPQs = \frac{F_m 24h - F_m}{F_m} \quad (6a)$$

$$NPQt = NPQd + NPQs \quad (6b)$$

where F_m and F_m' are the maximum fluorescence of dark and light (incubation-irradiance) acclimated cells, respectively, and F_m24h is the maximum fluorescence of dark-acclimated cells for 24 hours to allow complete relaxation of NPQs. NPQ calculations were computed with the 30 seconds RLC protocol. To calculate the maximum non-photochemical quenching (NPQmax) and developed NPQ at 30 μmol photons m^{-2} s^{-1} (NPQ30), a function was fitted to the data by least-square fit according to Serôdio & Lavaud (2011):

$$NPQ\ (E)\ =\ NPQ_{max} \cdot \frac{E^n}{E_{50}^n + E^n} \quad (7)$$

where NPQmax is the maximum NPQ value, E50 is the irradiance at which 50% of NPQmax is reached and n is the Hill coefficient of the fit (the sigmoidicity of the curve).

^{14}C incubations

A sample was first collected for each culture, and inoculated with inorganic ^{14}C ($NaH^{14}CO_3$, 2 μCi ml^{-1}). Samples were then processed as described in Bruyant et al. (2005). Inoculated culture aliquots of 1 ml were dispensed into 24 glass scintillation vials of 7 ml cooled in separate thermo-regulated alveoli (0°C). The vials were exposed to 24 different light levels provided by separate LEDs (LUXEON Rebel, Philips lumileds) from the bottom of each alveolus. The PAR (E, μmol photons m^{-2} s^{-1}) in each alveolus was measured before incubation with a quantum sensor (Heinz Walz GmbH, US-SQL) equipped with a 4π collector. After 20 min of incubation, culture aliquots were fixed with 50 µL of buffered formalin then placed under the fume hood and acidified (250 µL of HCl 50%) for 3 hours to remove the excess inorganic carbon (JGOFS protocol, UNESCO 1994). Finally, 6 mL of scintillation cocktail (Ecolume, MP Biomedicals) were added to each vial prior to counting using a liquid scintillation counter (Perkin Elmer® Tri-Carb 2910TR). This step allowed determining the amount of radiolabeled carbon assimilated by the cells from the number of disintegration per minute (DPM). To determine the total amount (total activity) of bicarbonate added, three 20 μl aliquots of radioactive sample were added to 50 μl of an organic base (ethanolamine) and 6 ml of the scintillation cocktail into glass scintillation vials. The carbon fixation rate was finally computed according to Parsons et al. (1984)

$$P = \frac{(R_S - R_b) \cdot W}{R \cdot N} \quad (8)$$

where P is the rate of carbon fixation [mg C m^{-3} h^{-1}], R is the total activity (DPM), N is the number of hours of incubation, R_S is the sample count (DPM) corrected for quenching, R_B is the blank (or dark sample) count (DPM) corrected for quenching and W is the total weight of carbon dioxide available. The relationship between the rate of carbon fixation (P) and irradiance (E) was fitted to the equation determined by Platt et al. (1980) to obtain the photosynthetic coefficients:

$$P = P_S \left[1 - exp\left(-\frac{\alpha E}{P_S}\right)\right] exp\left(-\frac{\beta E}{P_S}\right) + P_0 \quad (9)$$

where P_S is the maximum carbon fixation rate in absence of photoinhibition [μg C m^{-3} h^{-1}], α is the initial slope of the carbon fixation *vs*. irradiance curve [μg C m^{-3} h^{-1} (μmol photons

m^{-2} $s^{-1})^{-1}$], E is the incubation irradiance (μmol photons m^{-2} s^{-1}), β is the photoinhibition coefficient [μg C m^{-3} h^{-1} (μmol photons m^{-2} $s^{-1})^{-1}$] and P_0 is the intercept of the curve [μg C m^{-3} h^{-1}]. The maximum carbon fixation rate at saturating irradiance (P_{max}) was calculated as follow:

$$P_{max} = P_S \left(\frac{\alpha}{\alpha+\beta}\right)\left(\frac{\beta}{\alpha+\beta}\right)^{\frac{\beta}{\alpha}} \quad (10)$$

Statistical analysis: mean comparison of parameters between sampling periods

Different time windows were considered to follow the evolution of the measured parameters. The time windows considered are those with large changes in tracked parameter levels. Generally, the full duration of a given phase of the experiment, e.g. 83 days of darkness (or 63 days for carbon fixation parameters), is the period considered for statistical comparison. In some cases, within a given phase, there was an apparent change in the direction of the variation, e.g. see the number of cell per ml that increases from 0 to 28 days of darkness and decreases after from 28 to 83 days of darkness (Fig. 2a). For a given parameter, the time at which this directional change occured splits a given phase of the experiment into two periods for statistical comparison, e.g. $D_{0\text{-}28}$ and $D_{28\text{-}83}$ for the number of cell per ml in the dark. For the dark period (D), there were four main periods considered: up to the first month ($D_{0\text{-}28}$), up to the second month ($D_{0\text{-}63}$), up to the third month ($D_{0\text{-}83}$) and between the first and the third months ($D_{28\text{-}83}$). For the light return periods (L1, L2), the periods used for comparisons are specified in the text relatively to time ranges of interest, e.g. from 30 minutes to three days of illumination ($L1_{30min\text{-}3d}$). To determine whether there was a significant variation in the measured parameters during the dark experiment, we used linear mixed models that included an error term (or random effect) on the culture to account for the pseudo-replication of the data. For the light return periods, the mixed effect models also included a fixed effect on the light experiments (whether it was the first or the second light return experiment) and an interaction term between the two fixed effects (time and experiment). To test for temporal autocorrelation for each measured parameter, models were compared including a first order autocorrelation structure or not. ΔAIC was computed between each paired model to determine if the two models showed equivalent power or not. The models were considered equivalent if ΔAIC < 5 and the model without a first

autocorrelation structure was then chosen. For ΔAIC > 5, the model with the lowest AIC was chosen (supplementary files, model_significance_dark & model_significance_light). Temporal autocorrelation was found to be present only rarely and was accounted for when necessary. The linear mixed-effects models were fitted in R using the nlme package v3.1-137 (Pinheiro et al. 2018). All statistical analyze were performed in R 3.5.2 (R Core Team 2018). The complete and detailed statistical results are provided in supplementary files. The p-values reported in the text are those for the parameters relative change for the considered periods (supplementary files, posthoc_comparisons_dark & posthoc_comparisons_light) or those for the interaction term between time and experiment to determine if a parameter's variations for both light return periods are similar to each other or not (model_significance_light). The figures presented in the Results and Discussion section show Dark, Light return 1 and Light return 2 data altogether to provide a visual comparison between the three experiments. Light return 1 and Light return 2 data are enlarged in supplementary figures to allow easier comparison between each other. The lines between sampling periods are strictly shown for visual clarity and do not imply interpolated levels of any parameters. The mean values and standard deviations plotted in these figures are available for the main sampling periods in Table S1, S2 and S3.

Results & Discussion

Prolonged darkness exposure to mimic the polar night

Light acclimated cultures of *F. cylindrus* were exposed to complete darkness over a period of three months to mimic the polar night. Multiple physiological processes were monitored for the first time in a dark experiment to such an extent on the model polar diatom *F. cylindrus*. The results are discussed with respect to earlier findings on polar and non-polar species to understand diatom dark survival in polar environments.

Cell and reserves

Cell number per ml of algal culture (Fig. 2a) increased slightly but significantly during the first month of the dark period by 27% ($D_{0\text{-}28}$, P-value = 4.26×10^{-3}), which is likely due to a final cell division for a subset of the cell population at the beginning of the dark period. For the same period, the culture biovolume (Fig. 2a) did not increase significantly ($D_{0\text{-}28}$, P-value = 1.05×10^{-1}) because the average cell volume significantly decreased by 8% ($D_{0\text{-}28}$, P-value = 1.08×10^{-2}) as a consequence of cell division (Fig. 2b). The cell number and the biovolume then decreased until the end of the third month of darkness, although not significantly ($D_{28\text{-}83}$, $P\text{-value}_{\text{cell number}} = 1.06 \times 10^{-1}$, $P\text{-value}_{\text{biovolume}} = 1.38 \times 10^{-1}$), to end up at values slightly above the t0 (values just before dark transition). During the first month of darkness, the carbon cell quota significantly decreased by 34% ($D_{0\text{-}28}$, P-value = 3.57×10^{-3}) (Fig. 2c). The Carbon cell quota then significantly increased until the end of the third month ($D_{28\text{-}83}$, P-value = 5.19×10^{-4}) to values slightly above the t0. The variations in the nitrogen cell quota were similar to those of cellular carbon but none of the comparisons were significant ($D_{0\text{-}28}$, P-value = 1.11×10^{-1}; $D_{28\text{-}83}$, P-value = 9.02×10^{-2}).

A potential mechanism for long-term dark survival is to lower metabolism and to fine-tune the utilization rate of stored energy products (Handa 1969; Palmisano & Sullivan 1982; Dehning & Tilzer 1989; Jochem 1999; Popels et al. 2007; Schaub et al. 2017). In our experiment, the carbon cell quota did decrease for the first month of the dark period. However, this decrease was likely the consequence of cell division on cell volume. Indeed, the particulate organic carbon concentration per ml of culture did not decrease significantly

during the first month ($D_{0\text{-}28}$, P-value = 1.58×10^{-1}) (Fig. S7). The lipid droplets cell quota probed with BODIPY (RFU) remained mostly constant within the first month with a slight but significant increase of 5% ($D_{0\text{-}28}$, P-value = 1.18×10^{-2}) (Fig. 2b). Lipid droplets then slowly and significantly decreased until the end of the third month in the dark by 11% ($D_{28\text{-}83}$, P-value = 1.14×10^{-5}). Hence, this suggests very low dark metabolic rates and low energy reserve consumption as a survival process in *F. cylindrus*. The study by Mock et al. (2017) on the *F. cylindrus* transcriptome response to 7 days of darkness showed that metabolic activities were largely suppressed with approximately 60% of all genes down-regulated. However, genes involved in starch, sucrose and lipid metabolism were up-regulated, which likely fuelled the remaining metabolic needs within the cell for this short period of darkness. It is common that the rate of energy consumption is high in the first weeks of darkness, but decreases as the cells age in darkness (Handa 1969; Dehning & Tilzer 1989; Popels et al. 2007; Schaub et al. 2017). The results of the present study show a more stable pattern in the carbon, nitrogen and lipid droplets quotas, which is in agreement with global metabolism suppression over a long period of darkness. This global metabolism suppression could also be due, to some extent, to the colder temperature at which polar species grow. The rate of energy reserve depletion is likely to be lower for polar species, despite adaptations that compensate for lower kinetics at low temperature (Lyon & Mock 2014), and may contribute to longer darkness survival for polar species than for temperate species as observed by Peters (1996).

The minor increase of the carbon quota after 1 month was unexpected. Note that if bacterial presence and growth were to account for this increase, a sufficient amount of dissolved organic carbon (DOC) would have had to be initially present in the culture medium to sustain heterotrophic bacterial growth (Rivkin & Anderson 1997). The cultures were axenically handled and the fresh culture medium was initially free of DOC. It is unlikely that DOC was released from broken cells by the magnetic stirrer because the cell number remained quite steady through the full length of the experiment. Despite the minor increase in cellular carbon toward the end of the dark experiment, the general trend of the cell reserves data supports the interpretation of a suppression of metabolic activity in the dark.

Photosynthetic apparatus dismantlement

When cells are exposed to a long period of darkness, the photosynthetic machinery is not operating to convert light to chemical energy. A metabolic cost is associated with sustaining the molecular components of the photosynthetic apparatus (Geider & Osborne 1989; Quigg & Beardall 2003; Li et al. 2015). Based on the assumption of a lower metabolism and slower protein turnover in darkness (Li et al. 2016), renewal of degraded photosynthetic components should be limited. Hence, Chl*a* and the main photosynthetic accessory pigment Fucoxanthin (Fuco) cell quotas decreased as in past experiments (Peters & Thomas 1996; Baldisserotto et al. 2005a; Veuger & van Oevelen 2011). Chl*a* and Fuco decreased significantly after 3 months of darkness by 41% and 48% respectively ($D_{0\text{-}83}$, P-value$_{Chla}$ = 6.88 x 10^{-3}, P-value$_{Fuco}$ = 1.27 x 10^{-3}) (Fig. 3a). For the same period, the photoprotective pigments (Diadinoxanthin (DD) + Diatoxanthin (DT)) cell quotas decreased, although not significantly, by 20% ($D_{0\text{-}83}$, P-value = 4.51 x 10^{-1}). The pool decrease was attributable to the DD form since DT fully returned to its epoxidized form (DD) after 1 day of darkness (Fig. 3b). Thus, the photosynthetic (Chl*a* + Chl*c* +Fuco) to photoprotective pigments ratio decreased significantly by 31% ($D_{0\text{-}83}$, P-value = 4.31 x 10^{-6}) (Fig. 3c). As a likely consequence of this specific pigment degradation, σ_{PSII} decreased significantly by 27% ($D_{0\text{-}83}$, P-value = 1.41 x 10^{-4}) (Fig. 3c).

Photosynthetic proteins cell quotas (PsbA and RbcL) decreased significantly after 3 months of darkness ($D_{0\text{-}83}$) by 85% and 72% respectively ($D_{0\text{-}83}$, P-value$_{PsbA}$ = 2.03 x 10^{-4}, P-value$_{RbcL}$ = 1.44 x 10^{-4}). They reached a much lower detected level relative to t0 than did the photosynthetic pigments (Fig. 4a). The massive decrease for PsbA is indicative of a PSII core complex degradation as seen in other experiments with a green chlorophyte and a snow xanthophycean algae (Baldisserotto et al. 2005a; Baldisserotto et al. 2005b; Ferroni et al. 2007) under prolonged darkness. Based on the photosynthetic proteins results, one would expect that carbon fixation capacity was largely suppressed in absence of these key proteins, particularly RbcL. Indeed, the carbon fixation *vs*. irradiance curves showed a major significant decrease within 2 months in α and in P_{max} per cell by 92% and 98% respectively ($D_{0\text{-}63}$, P-value$_{\alpha}$ = 1.16 x 10^{-3}, P-value$_{Pmax}$ = 4.58 x 10^{-6}) (Figs. 4b,c) (Fig. 5a),

as reported before (Hellebust & Terborgh 1967; Dehning & Tilzer 1989; Peters & Thomas 1996; Popels et al. 2007; Kvernvik et al. 2018; Lacour et al. 2019). P_{max} per cell decreased faster than the RbcL cell quota, possibly because of an early inactivation of the carbon fixation enzyme (Hellebust & Terborgh 1967; MacIntyre et al. 1997; Lacour et al. 2019). Interestingly, in the study of Lacour et al. (2019), the RuBisCO-to-carbon ratio did not change for cultures of *Chaetoceros neogracile* exposed to 1 month of darkness, despite a strong decrease in P_{max} per carbon. Note that the RbcL cell quota in our study also did not decrease significantly during the first month in darkness ($D_{0\text{-}28}$, P-value = 5.41×10^{-1}) before it began to decrease, which suggest that an initial decrease in RuBisCO activity, rather than its pool, explains the initial decrease in P_{max}. Modification of the carbon fixation enzyme to an inactive state may be triggered by dark transition (Parry et al. 2008). P_{max} also decreased faster relative to α, which significantly lowered the light saturation parameter E_k by 72% ($D_{0\text{-}63}$, P-value = 5.38×10^{-4}) (P_{max}/α, Fig. S10). This decrease of E_k during prolonged darkness increased the risk of photoinhibition upon subsequent re-illumination, because a given re-illumination level would rise farther above E_k, resulting in excess excitation. The photoprotective NPQ (Eqn 5) was indeed induced even for the lowest RLC irradiances, most likely because of impaired electron sink capacities such as carbon fixation (Huner et al. 1998; Joliot & Alric 2013) (Fig. S11).

While the carbon fixation curve parameters decreased, Φ_M (Eqn 1) showed no significant variation after three months of darkness ($D_{0\text{-}83}$, P-value = 9.96×10^{-1}) even though a decrease has previously been observed in prolonged darkness in diatoms (Reeves et al. 2011; Martin et al. 2012; Lacour et al. 2019) (Fig. 4b). The internally normalized fluorescence ratio Φ_M reflects the photochemical activity of the remaining PSII capable of at least a single turnover within the remaining pool of viable cells. But the PsbA determinations (Fig. 4a) show that the content of PSII decreased significantly. Analyses of rETRmax (Fig. 4c) also that electron transport away from the remaining PSII was also suppressed. Note that the drop in rETRmax is not available in Fig. 4c because no measurements were made during the first two weeks of the dark period (see Materials & Methods, sampling design). Nevertheless, together with P_{max}, Fig. 4c strongly suggests that rETRmax was high before the dark transition. Thus, the combination of the drop in PSII

content and the drop in rETRmax can together explain the drop in carbon fixation curve parameters. Furthermore, the ^{14}C incubations lasted 20 minutes. Viable cells taken out of an extended period of darkness and exposed to ^{14}C incubations may suffer more from impaired electron sink capacities than during a nearly instantaneous measurement of photochemical activity using a single saturating flash.

Light exposure after darkness

The dark acclimated *F. cylindrus* cultures were re-exposed to light after 1.5 months and after 3 months of darkness and monitored for the same physiological parameters. Previous experiments that studied the light transition from prolonged darkness in polar diatoms are scarce. However, Kvernik et al. (2018) and Lacour et al. (2019) recently studied the ability of dark acclimated polar phytoplankton communities and *Chaetoceros neogracile* culture, respectively, to resume photophysiolocal activity and cell growth over a wide range of irradiance. We found results consistent with their studies, with the addition of other physiological and metabolic features that complement our understanding of the acclimation processes at stake for polar night survival and return to light.

Photosensitivity and photosynthetic apparatus reassembly

F. cylindrus cells acclimated to darkness largely dismantled key catalytic complexes of their photosynthetic apparatus, while retaining much of their pigment bed. To limit photo-damage, diatoms mainly rely on NPQ mediated by the xanthophyll cycle (Lavaud & Goss 2014), especially for *F. cylindrus* growing at low temperatures, which limits other physiological responses (Petrou et al. 2010, Petrou et al. 2011). Given the low photosynthetic capacities reached during the dark period, a rapid NPQ response was expected to occur immediately upon light return to dissipate excessive excitation. For the Light return 1 experiment, the highest NPQ30 was indeed observed immediately upon re-illumination (Fig. 6a). This level of NPQ significantly decreased by 69% to 'a steady state' within 3 days of re-illumination ($L1_{30min-3d}$, P-value = 5.43×10^{-11}). The de-epoxidation state (DES: DT/(DD+DT)) showed consistent variations (64% significant decrease, $L1_{30min-3d}$, P-value = 2.35×10^{-3}) indicating that NPQ was mostly related to DT (Lavaud & Goss

580 2014) (Fig. 6a). The NPQ30 was close to the NPQmax induced during the RLC (at 111
581 μmol photons m^{-2} s^{-1}, Fig. S11).
582 In the Light return 2 experiment, the NPQ induction showed a different pattern. Despite the
583 presence of DT (Fig. 3b), NPQ remained low (Fig. 6b). This particular inconsistency
584 between DT synthesis and NPQ has previously been observed with *Phaeodactylum*
585 *tricornutum* (Lavaud & Kroth 2006; Lavaud & Lepetit 2013) and *F. cylindrus* (Kropuenske
586 et al. 2009). According to Kropuenske *et al.* (2009), 30 minutes of dark-acclimation before
587 the NPQ measurements are not sufficient to achieve complete re-epoxidation of DT for
588 highly light-stressed cells, so that NPQ remains 'locked-in' and relaxes only over several
589 hours (Lavaud & Goss 2014). To allow this sustained part of NPQ to relax, extra samples
590 were dark acclimated for 24 hours to calculate NPQt (Eqn 6a, 6b). NPQt developed at 30
591 μmol photons m^{-2} s^{-1} was higher after 2 hours, 5 hours and 1 day, but not after 30 minutes
592 of re-illumination (Fig. S11). Possibly, for this short timing, the PSII light-harvesting
593 system was still too dismantled to activate a fully dynamic NPQ response immediately
594 upon re-illumination.
595
596 In the Light return 1 experiment, Chl*a* and Fuco cell quotas first decreased over 3 days of
597 re-illumination, although not significantly ($L1_{30min\text{-}3d}$, $P\text{-value}_{Chla} = 9.96 \times 10^{-1}$, $P\text{-value}_{Fuco}$
598 $= 7.76 \times 10^{-2}$) (Fig. 3a). The simultaneous decrease of Chl*a* and Fuco and significant
599 increase of DD cell quota ($L1_{30min\text{-}3d}$, P-value $= 2.05 \times 10^{-4}$) (Fig. 3b) led in turn to a
600 significant 43% decrease of the Photosynthetic/Photoprotective pigment ratio until the third
601 day of the Light return 1 experiment ($L1_{30min\text{-}3d}$, P-value $= 4.01 \times 10^{-5}$) (Fig. 3c). After 3
602 days, photosynthetic pigments stopped decreasing and started to build up as previously
603 observed in past experiments on polar and non-polar diatoms (Griffiths 1973; Peters &
604 Thomas 1996; Nymark et al. 2013). The late build-up of photosynthetic pigments, although
605 not achieving statistical significance ($L1_{3d\text{-}6d}$, $P\text{-value}_{Chla} = 8.32 \times 10^{-2}$, $P\text{-value}_{Fuco} = 5.56 \times$
606 10^{-2}), stabilised the Photosynthetic/Photoprotective pigment ratio until the 6^{th} day of the
607 Light return 1 experiment ($L1_{3d\text{-}6d}$, P-value $= 5.90 \times 10^{-1}$).
608 In the Light return 2 experiment, variations in Chl*a* and Fuco cell quotas were not
609 significantly different to the Light return 1 experiment according to the interaction terms

610 (P-value $_{Chla}$ = 8.21 x 10^{-2}, P-value$_{Fuco}$ = 7.63 x 10^{-2}) (Fig. 3a), but DD cell quota did not
611 increase similarly as in the Light return 1 experiment and thus was significantly different,
612 (P-value$_{DD}$ = 2.96 x 10^{-4}) (Fig. 3b). Nevertheless, in both light experiments, the
613 Photosynthetic/Photoprotective pigment ratio significantly decreased until the 6th day of
614 light exposure by 30% and 35% respectively ($L1_{30min-6d}$, P-value = 5.34 x 10^{-3} / $L2_{30min-6d}$,
615 P-value = 2.19 x 10^{-3}) (Fig. 3c). Thus, the pigment composition of the light harvesting
616 antennae shifted gradually to a higher proportion of xanthophylls (DD+DT), typical of high
617 light acclimated algal cells (MacIntyre et al. 2002; Kropuenske et al. 2009; Lepetit et al.
618 2013). The σ_{PSII} variations were similar to Photosynthetic/Photoprotective pigment,
619 although not decreasing significantly ($L1_{30min-6d}$, P-value = 9.92 x 10^{-1} / $L2_{30min-6d}$, P-value =
620 1.39 x 10^{-1}) (Fig. 3c), and are in agreements with the observations by Kvernvik et al. (2018)
621 on Arctic microalgae communities.
622
623 The abundance of photosynthetic proteins PsbA and RbcL increased during the Light return
624 1 experiment (Fig. 4a). The PsbA cell quota remained stable within the first 5 hours
625 ($L1_{30min-5h}$, P-value = 1.00 x 10^{0}), consistent with rapidly-induced photoprotection
626 protecting a further degradation of PsbA (Wu et al. 2011). It then significantly increased
627 until the 6th days ($L1_{5h-6d}$, P-value = 2.86 x 10^{-8}) to end up near t0 values, supporting a
628 reassembly of the PSII reaction center (RCII) back to the pre-acclimation state. The RbcL
629 cell quota was nearly undetectable within the first day, but then increased significantly into
630 a quantifiable range until the 6th day ($L1_{1d-6d}$, P-value = 2.38 x 10^{-14}) (Fig. 4a). However,
631 P_{max} per cell increased significantly within 1 day of light exposure ($L1_{dark-1d}$, P-value = 1.54
632 x 10^{-8}, much of the increase occurred between the previously measured dark level (D_{28}) and
633 the first 30 minutes of illumination) (Fig. 4c) (Fig. 5b) as also observed by Popels et al.
634 (2007). The discrepancies with the apparent delayed recovery of RbcL content results from
635 RbcL in darkness and early re-illumination falling below a quantifiable range. Indeed, the
636 low residual content of RuBisCO would operate at maximal activity within 1 day of light
637 exposure (MacIntyre et al. 1996; MacIntyre et al. 1997). Φ_M also increased rapidly within 1
638 day of light exposure ($L1_{30min-1d}$, P-value = 9.55 x 10^{-6}) (Fig. 4b), supporting a fast recovery
639 of the photophysiology (Luder et al. 2002; Kvernvik et al. 2018; Lacour et al. 2019).

Despite the slow synthesis of photosynthetic proteins and the decrease of the Photosynthetic/Photoprotective pigment ratio, the cells achieved efficient coupling from RCII photochemistry to carbon fixation within 1 day in the Light return 1 experiment.

In the Light return 2 experiment, PsbA and RbcL cell quotas were initially nearly undetectable. The recovery slopes of P_{max} per cell and Φ_M appeared lower and are significantly different from those in the Light return 1 experiment according to the interaction terms (P-value$_{Pmax}$ = 7.32 x 10^{-6}, P-value$_{\Phi M}$ = 5.79 x 10^{-9}) (Figs. 4b,c). The recovery in the Light return 2 experiment was possibly slowed by a more extensive dismantling of the photosynthetic apparatus and electron sink capacities, and by a likely substantial population of dead cells under longer darkness acclimation (3 months vs. 1.5 months). As in the dark experiment, the variations in Φ_M likely reflected the fluorescence ratio recovery within the PSII pool of remaining viable cells, while P_{max} reflected the whole cell population (including dead cells and empty frustules). Thus, the speed of recovery was indeed lower in the Light return 2 experiment as shown by the variations in Φ_M.

Metabolic recovery

All together the cells rapidly (within 1 day) acclimated to the applied irradiance (30 μmol photons m^{-2} s^{-1}) in the Light return 1 experiment, as illustrated by the rapid significant increase of E_k ($L1_{dark\text{-}1d}$, P-value = 2.95 x 10^{-5}, much of the increase occurred between the previously measured dark level (D_{28}) and the first 30 minutes of illumination) (Fig. S10). The interaction term is also not significant for E_k, meaning that the increases in E_k for the Light return experiments 1 and 2 are statistically equivalent (P-value = 1.44 x 10^{-1}). Lacour et al. (2019) also measured a rapid increase in E_k and rETRmax within the first hours of light return for *Chaetoceros neogracile* cultures exposed to 4 different re-illumination levels (5, 27, 41 and 154 μmol photons m^{-2} s-1) with a more rapid recovery for higher light levels. Kvernvik et al. (2018) also measured a similar fast recovery in photophysiology on Arctic microalgal communities for low and high re-illumination levels (1 and 50 μmol photons m^{-2} s-1). In the present study, the time at which E_k matches the actual irradiance the cells were exposed to during light returns testifies to their full ability to perform photochemistry and fix carbon to support anabolism and ultimately cell growth, particularly during the Light return 1 experiment.

Carbon and nitrogen cell quotas increased significantly by 62% and 66%, respectively, over 6 days for the Light return 1 experiment ($L1_{30min\text{-}6d}$, P-value$_{carbon}$ = 1.12 x 10^{-2}, P-value$_{nitrogen}$ = 2.10 x 10^{-6}) (Fig. 2c). The lipid droplets cell quota also significantly increased by 14% in 6 days ($L1_{5h\text{-}6d}$, P-value = 3.85 x 10^{-6}) (Fig. 2b). However, carbohydrates probably accounted for some of the increase in carbon quotas (Myklestad 1974; Chauton et al. 2013) despite the lack of carbohydrates data to support this statement. The cell volume significantly increased by 31% in 6 days ($L1_{30min\text{-}6d}$, P-value = 1.19 x 10^{-11}) (Fig. 2b) which is consistent with a larger content in lipids, carbon and nitrogen. As expected, the cell population entered an exponential growth phase measured between 1 day and 6 days following exposure to light with a mean population growth rate of 0.146±0.010 d^{-1} (Fig. 2a). This was 40% lower than the mean growth rate measured during the pre-darkness acclimation period (0.244±0.041 d^{-1}), possibly as a consequence of the larger size of new cells and of potential mortality before and during light return. For the Light return 2 experiment, the increase in the carbon cell quota was statistically equivalent to the Light return 1 experiment as supported by the interaction term (P-value = 1.28 x 10^{-1}) while nitrogen cell quota, lipid droplets cell quota, cell volume and cell number per ml of algal culture slopes were significantly different from the Light return 1 experiment (P-value$_{nitrogen}$ = 7.28 x 10^{-5}, P-value$_{lipid}$ = 2.34 x 10^{-2}, P-value$_{cell\ volume}$ = 3.12 x 10^{-11}, P-value$_{cell\ number}$ = 1.38 x 10^{-7}) (Figs. 2a,b,c). Cell growth was not observed over the Light return 2 tracked re-illumination period. Along with the greater dismantling of the photosynthetic apparatus impacting the speed of photophysiological recovery, mortality may have compromised the population ability to reinitiate detectable growth upon light exposure. Nevertheless, a fraction of the population recovered as the Φ_M data suggest that living cells recovered function of the PSII pool after ~ 3 days in Light return 2 (Fig. 4b). For parameters that showed a lag phase, that lag phase may be in fact only apparent, because those parameters were normalized to the total number of cells (including the dead ones). As healthy cells divide and the relative contribution of dead cells thereby decreases, full population recovery may be observed. The lag phase was previously reported to increase with increasing previous dark period (Dehning & Tilzer 1989; Peters & Thomas 1996). In antarctic diatoms, the lag phase lasted 4 days following 74 days in the dark (Peters &

700 Thomas 1996). The results of the present experiment suggest that *F. cylindrus* had a lag
701 phase longer than 6 days before reaching detectable exponential growth after 3 months of
702 darkness, yet recovery of exponential growth could not be confirmed within the timescale
703 of our measures.

Conclusions

F. cylindrus achieved a physiological resting state a few days following the transition to dark and maintained it throughout until the return to light (Fig. 7). This rather stable state was characterized by very low consumption of energy reserves, a slow decrease of photosynthetic pigments, a faster decrease in key photosynthetic protein complexes, and very low photosynthetic capacities. Subsequent transition back to light after 1.5 months first triggered fast photoprotection followed by the renewal of photosynthetic components. Rapid recovery of photophysiology occurred within a few hours of return to light, followed by resumption of cell growth after 1 day of re-illumination. The re-acclimated light state showed similar characteristics to high light grown cells regarding the changes in pigment composition, at least over the initial 6 days. The results from the transition to light after 3 months highlighted an apparent lag phase that increases in length with longer periods of darkness. Mortality in the dark may have delayed the full recovery of the population with an apparent lag phase longer than 6 days.

The results of this study suggest that the low rate of energy consumption for dark survival and high photoprotective capacity upon light return may be two physiological traits that help *F. cylindrus* to thrive in polar oceans. It remains to be investigated whether mortality or sustained down regulation, or both, are the major factor(s) explaining the stronger physiological drop-down and the delayed recoveries of measured physiological and molecular parameters after prolonged darkness (3 months). Progressive dark and light transitions, rather than sudden shifts as in this experiment, should also be tested and coupled with mortality measurements to determine if a particular light return regime compromises survival more than another one. The role of heterotrophy in dark survival remains to be clarified, because available dissolved organic carbon within and underneath sea-ice (Riedel et al. 2008) could potentially improve diatom survival to the winter polar night. Finally, the expression of genes was not within the scope of this study and should also be addressed in future experiments to uncover the signature of metabolic pathways over a dark period that is significant to the Arctic polar night.

Acknowledgements

The authors thank Catherine Lalande and Thibaud Dezutter for their help with the CHN analyzer, Marie-Josée Martineau for her help with pigment analysis, Gabrièle Deslonchamps for her help with the culture media nutrients analysis, Alexandre Dubé and Chris Eberlein for their help with the flow cytometer, Marc-André Lemay for his help with R programming, José Lagunas-Morales and Guislain Bécu for their help with the illumination system of the CARON growth chamber and Nicolas Schiffrine for his help with algal culturing. This work was supported through NSERC Discovery, Fonds de recherche du Québec – Nature et technologies and Canada Excellence Research Chair in Remote Sensing of Canada New Arctic Frontier (M. Babin), and through a Canada Research Chair in Phytoplankton Ecophysiology, the Canada Innovation Foundation and the New Brunswick Innovation Foundation (D. A. Campbell).

Authors Contribution

Morin P. I. is the main author of this work with major contributions to designing and running the experiments, analysing the data and writing the paper. All co-authors helped with running the experiments and/or revising the paper. Campbell D. A., J. Lavaud and M. Babin helped with the structure of the manuscript and the discussion of the data.

751 *References*

752

753 Anderson O. R. 1975. The ultrastructure and cytochemistry of resting cell formation in
754 *Amphora coffaeformis* (Bacillariophyceae). Journal of Phycology **11**: 272-281.
755 Antia N. J. 1976. Effects of temperature on darkness survival of marine microplanktonic
756 algae. Microbial Ecology **3**: 41-54.
757 Ardyna, M., M. Babin, M. Gosselin, E. Devred, S. Belanger, A. Matsuoka, and J. E.
758 Tremblay. 2013. Parameterization of vertical chlorophyll a in the Arctic Ocean:
759 impact of the subsurface chlorophyll maximum on regional, seasonal, and annual
760 primary production estimates. Biogeosciences **10**: 4383-4404.
761 Baldisserotto, C., L. Ferroni, C. Andreoli, M. P. Fasulo, A. Bonora, and S. Pancaldi. 2005a.
762 Dark acclimation of the chloroplast in *Koliella antarctica* exposed to a simulated
763 austral night condition. Arctic Antarctic and Alpine Research **37**: 146-156.
764 Baldisserotto, C., L. Ferroni, I. Moro, M.P. Fasulo, and S. Pancaldi. 2005b. Modulations of
765 the thylakoid system in snow xanthophycean alga cultured in the dark for two
766 months: comparison between microspectrofluorimetric responses and
767 morphological aspects. Protoplasma **226**: 125-135.
768 Brennan, L., A. B. Fernández, A. S. Mostaert, and P. Owende. 2012. Enhancement of
769 BODIPY 505/515 lipid fluorescence method for applications in biofuel-directed
770 microalgae production. Journal of Microbiological Methods **90**: 137-143.
771 Bruyant, F., and others. 2005. Diel variations in the photosynthetic parameters of
772 *Prochlorococcus* strain PCC 9511: Combined effects of light and cell cycle.
773 Limnology and Oceanography **50**: 850-863.
774 Chauton, M. S., P. Winge, T. Brembu, O. Vadstein, and A. M. Bones. 2013. Gene
775 regulation of carbon fixation, storage, and utilization in the diatom *Phaeodactylum*
776 *tricornutum* acclimated to light/dark cycles. Plant Physiology **161**: 1034-1048.
777 Cullen, J. J., and M. R. Lewis. 1988. The kinetics of algal photoadaptation in the context of
778 vertical mixing. Journal of Plankton Research **10**: 1039-1063.
779 Dehning, I., and M. M. Tilzer. 1989. Survival of *Scenedesmus acuminatus* (Chlorophyceae)
780 in darkness. Journal of Phycology **25**: 509-515.
781 Doucette G. J., and G. A. Fryxell. 1983. *Thalassiosira antarctica*: vegetative and resting
782 stage chemical composition of an ice-related marine diatom. Marine Biology **78**: 1-
783 6.
784 Eilers, P. H., and J. C. H. Peeters. 1988. A model for the relationship between light
785 intensity and the rate of photosynthesis in phytoplankton. Ecological Modelling **42**:
786 199-215.
787 Ferroni, L., C. Baldisserotto, V. Zennaro, C. Soldani, M. P. Fasulo, and S. Pancaldi. 2007.
788 Acclimation to darkness in the marine chlorophyte *Koliella antarctica* cultured
789 under low salinity: hypotheses on its origin in the polar environment. European
790 Journal of Phycology **42**: 91-104.
791 Geider, R. J., and B. A. Osborne. 1989. Respiration and microalgal growth: a review of the
792 quantitative relationship between dark respiration and growth. New Phytologist
793 **112**: 327-341.

794 Godhe, A., and K. Härnström. 2010. Linking the planktonic and benthic habitat: genetic
795 structure of the marine diatom *Skeletonema marinoi*. Molecular Ecology **19**: 4478-
796 4490.
797 Griffiths, D. J. 1973. Factors affecting the photosynthetic capacity of laboratory cultures of
798 the diatom *Phaeodactylum tricornutum*. Marine Biology **21**: 91-97.
799 Guillard, R. R. L., and P. E. Hargraves. 1993. *Stichochrysis immobilis* is a diatom, not a
800 chrysophyte. Phycologia **32**: 234-236.
801 Handa, N. 1969. Carbohydrate metabolism in the marine diatom *Skeletonema costatum*.
802 Marine Biology **4**: 208-214.
803 Härnström, K., M. Ellegaard, T. Andersen, and A. Godhe. 2011. Hundred years of genetic
804 structure in a sediment revived diatom population. Proceedings of the National
805 Academy of Sciences **108**: 4252-4257.
806 Hellebust J. A., and J. Lewin 1977. Heterotrophic nutrition, p. 169-197. In: Burnett J. H.,
807 H. G. Baker, H. Beevers, and F. R. Whatley [eds.], The biology of diatoms.
808 University of California Press.
809 Hellebust, J. A., and J. Terborgh. 1967. Effects of environmental conditions on the rate of
810 photosynthesis and some photosynthetic enzymes in *Dunaliella tertiolecta* Butcher.
811 Limnology and Oceanography **12**: 559-567.
812 Horner, R., and V. Alexander 1972. Algal population in Arctic sea ice: an investigation of
813 heterotrophy. Limnology and Oceanography **17**: 454-458.
814 Huner, N. P. A., G. Oquist, and F. Sarhan. 1998. Energy balance and acclimation to light
815 and cold. Trends in Plant Science **3**: 224-230.
816 Jochem, F. J. 1999. Dark survival strategies in marine phytoplankton assessed by
817 cytometric measurement of metabolic activity with fluorescein diacetate. Marine
818 Biology **135**: 721-728.
819 Joliot, P., and J. Alric. 2013. Inhibition of CO_2 fixation by iodoacetamide stimulates cyclic
820 electron flow and non-photochemical quenching upon far-red illumination.
821 Photosynthesis Research **115**: 55-63.
822 Kolber, Z. S., O. Prasil, and P. G. Falkowski. 1998. Measurements of variable chlorophyll
823 fluorescence using fast repetition rate techniques: defining methodology and
824 experimental protocols. Biochimica Et Biophysica Acta-Bioenergetics **1367**: 88-
825 106.
826 Kropuenske, L. R., M. M. Mills, G. L. van Dijken, S. Bailey, D. H. Robinson, N. A.
827 Welschmeyer, and K. R. Arrigo. 2009. Photophysiology in two major Southern
828 Ocean phytoplankton taxa: photoprotection in *Phaeocystis antarctica* and
829 *Fragilariopsis cylindrus*. Limnology and Oceanography **54**: 1176-1196.
830 Kvernvik, A. C., C. J. M. Hoppe, E. Lawrenz, O. Prášil, M. Greenacre, J. M. Wiktor, and E.
831 Leu. 2018. Fast reactivation of photosynthesis in arctic phytoplankton during the
832 polar night. Journal of Phycology **54**: 461-470.
833 Lacour T., P.I. Morin, T. Sciandra, N. Donaher, D. A. Campbell, J. Ferland, and M. Babin.
834 2019. Decoupling light harvesting, electron transport and carbon fixation during
835 prolonged darkness supports rapid recovery upon re-illumination in the Arctic
836 diatom *Chaetoceros neogracilis*. Polar Biology 1-13.

837 Lavaud, J., and R. Goss. 2014. The peculiar features of non-photochemical fluorescence
838 quenching in diatoms and brown algae, p. 421-443. In B. Demmig-Adams, G.
839 Garab, W. Adams III and Govindjee [eds.], Non-photochemical quenching and
840 energy dissipation in plants, algae and cyanobacteria. Springer.
841 Lavaud, J., and P. G. Kroth. 2006. In diatoms, the transthylakoid proton gradient regulates
842 the photoprotective non-photochemical fluorescence quenching beyond its control
843 on the xanthophyll cycle. Plant and Cell Physiology **47**: 1010-1016.
844 Lavaud, J., and B. Lepetit. 2013. An explanation for the inter-species variability of the
845 photoprotective non-photochemical chlorophyll fluorescence quenching in diatoms.
846 Biochimica Et Biophysica Acta-Bioenergetics **1827**: 294-302.
847 Lefebvre, S., J. L. Mouget, and J. Lavaud. 2011. Duration of rapid light curves for
848 determining the photosynthetic activity of microphytobenthos biofilm *in situ*.
849 Aquatic Botany **95**: 1-8.
850 Lepetit, B., S. Sturm, A. Rogato, A. Gruber, M. Sachse, A. Falciatore, P. G. Kroth, and J.
851 Lavaud. 2013. High light acclimation in the secondary plastids containing diatom
852 *Phaeodactylum tricornutum* is triggered by the redox state of the plastoquinone
853 pool. Plant Physiology **161**: 853-865.
854 Leu, E., C. J. Mundy, P. Assmy, K. Campbell, T. M. Gabrielsen, M. Gosselin, T. Juul-
855 Pedersen, and R. Gradinger. 2015. Arctic spring awakening – Steering principles
856 behind the phenology of vernal ice algal blooms. Progress in Oceanography **139**:
857 151-170.
858 Lewin J. C. 1953. Heterotrophy in diatoms. Journal of General Microbiology **9**: 305-313.
859 Li, G., C. M. Brown, J. A. Jeans, N. A. Donaher, A. McCarthy, and D. A. Campbell. 2015.
860 The nitrogen costs of photosynthesis in a diatom under current and future pCO_2.
861 New Phytologist **205**: 533-543.
862 Li, G., and D. A. Campbell. 2013. Rising CO_2 Interacts with growth light and growth rate
863 to alter photosystem II photoinactivation of the coastal diatom *Thalassiosira*
864 *pseudonana*. PLOS ONE **8**: e55562.
865 Li, G., A. D. Woroch, N. A. Donaher, A. M. Cockshutt, and D. A. Campbell. 2016. A hard
866 day's night: diatoms continue recycling photosystem II in the dark. Frontiers in
867 Marine Science **3**: 218
868 Luder, U. H., C. Wiencke, and J. Knoetzel. 2002. Acclimation of photosynthesis and
869 pigments during and after six months of darkness in *Palmaria decipiens*
870 (Rhodophyta): a study to simulate Antarctic winter sea ice cover. Journal of
871 Phycology **38**: 904-913.
872 Lyon, B. R., and T. Mock. 2014. Polar microalgae: new approaches towards understanding
873 adaptations to an extreme and changing environment. Biology **3**: 56-80.
874 MacIntyre, H. L., and J. J. Cullen. 2005a. Using cultures to investigate the physiological
875 ecology of microalgae, p. 287-326. In R. A. Anderson [eds.], Algal culturing
876 techniques. Elsevier Academic Press.
877 MacIntyre, H. L., and J. J. Cullen. 2005b. Purification Methods for Microalgae, p. 177-132.
878 In R. A. Anderson [eds.], Algal culturing techniques. Elsevier Academic Press.

MacIntyre, H. L., R. J. Geider, and R. M. McKay. 1996. Photosynthesis and regulation of RuBisCO activity in net phytoplankton from Delaware Bay. Journal of Phycology **32**: 718-731.

MacIntyre, H. L., T. M. Kana, T. Anning, and R. J. Geider. 2002. Photoacclimation of photosynthesis irradiance response curves and photosynthetic pigments in microalgae and cyanobacteria. Journal of Phycology **38**: 17-38.

MacIntyre, H. L., T. D. Sharkey, and R. J. Geider. 1997. Activation and deactivation of ribulose-1,5-bisphosphate carboxylase/oxygenase (RuBisCO) in three marine microalgae. Photosynthesis Research **51**: 93-106.

Marshall, J., and F. Schott. 1999. Open-ocean convection: observations, theory, and models. Reviews of Geophysics **37**: 1-64.

Martin, A., A. McMinn, M. Heath, E. N. Hegseth, and K. G. Ryan. 2012. The physiological response to increased temperature in over-wintering sea ice algae and phytoplankton in McMurdo Sound, Antarctica and Tromso Sound, Norway. Journal of Experimental Marine Biology and Ecology **428**: 57-66.

McMinn, A., and A. Martin. 2013. Dark survival in a warming world. Proceedings of the Royal Society B-Biological Sciences **280**: 1-7.

McQuoid, M., A. Godhe, and K. Nordberg. 2002. Viability of phytoplankton resting stages in the sediments of a coastal Swedish fjord. European Journal of Phycology **37**: 191-201.

Mock, T., and others. 2017. Evolutionary genomics of the cold-adapted diatom *Fragilariopsis cylindrus*. Nature **541**: 536-540.

Mundy, C. J., D. G. Barber, and C. Michel. 2005. Variability of snow and ice thermal, physical and optical properties pertinent to sea ice algae biomass during spring. Journal of Marine Systems **58**: 107-120.

Myklestad, S. 1974. Production of carbohydrates by marine planktonic diatoms. I. Comparison of nine different species in culture. Journal of Experimental Marine Biology and Ecology **15**: 261-274.

Nymark, M., K. C. Valle, K. Hancke, P. Winge, K. Andresen, G. Johnsen, A. M. Bones, and T. Brembu. 2013. Molecular and photosynthetic responses to prolonged darkness and subsequent acclimation to re-illumination in the diatom *Phaeodactylum tricornutum*. PLOS ONE **8**: e58722.

Palmisano, A. C., and C. W. Sullivan. 1982. Physiology of sea ice diatoms. I. Response of 3 polar diatoms to a simulated summer-winter transition. Journal of Phycology **18**: 489-498.

Palmisano, A. C., and C. W. Sullivan. 1983. Physiology of sea ice diatoms. II. Dark survival of three polar diatoms. Canadian Journal of Microbiology **29**: 157-160.

Parry, M. A. J., A. J. Keys, P. J. Madgwick, A. E. Carmo-Silva, and P. J. Andralojc. 2008. RuBisCO regulation: a role for inhibitors. Journal of Experimental Botany **59**: 1569-1580.

Parsons, T. R., Y. Maita, and C. M. Lalli. 1984. Photosynthesis as measured by the uptake of radioactive carbon, p. 115-120. In T. R. Parsons [eds.], A manual of chemical & biological methods for seawater analysis. Pergamon Press.

Perrette, M., A. Yool, G. D. Quartly, and E. E. Popova. 2011. Near-ubiquity of ice-edge blooms in the Arctic. Biogeosciences **8**: 515-524.

Peters, E. 1996. Prolonged darkness and diatom mortality. II. Marine temperate species. Journal of Experimental Marine Biology and Ecology **207**: 43-58.

Peters, E., and D. N. Thomas. 1996. Prolonged darkness and diatom mortality I: Marine Antarctic species. Journal of Experimental Marine Biology and Ecology **207**: 25-41.

Petrou, K., M. A. Doblin, and P. J. Ralph. 2011. Heterogeneity in the photoprotective capacity of three Antarctic diatoms during short-term changes in salinity and temperature. Marine Biology **158**: 1029-1041.

Petrou, K., H. Ross, C. M. Brown, D. A. Campbell, M. A. Doblin, and P. J. Ralph. 2010. Rapid photoprotection in sea-ice diatoms from the East Antarctic pack ice. Limnology and Oceanography **55**: 1400-1407.

Pinheiro J., D. Bates, S. DebRoy, D. Sarkar and R Core Team. 2018. nlme: Linear and Nonlinear Mixed Effects Models. R package version 3.1-137, https://CRAN.R-project.org/package=nlme.

Platt, T., C. L. Gallegos, and W. G. Harrison. 1980. Photoinhibition of photosynthesis in natural assemblages of marine phytoplankton. Journal of Marine Research **38**: 687-701.

Popels L. C., and D. A. Hutchins. 2002. Factors affecting dark survival of the brown tide alga *Aureococcus anophagefferens* (Pelagophyceae). Journal of Phycology **38**: 738-744.

Popels, L. C., H. L. MacIntyre, M. E. Warner, Y. H. Zhang, and D. A. Hutchins. 2007. Physiological responses during dark survival and recovery in *Aureococcus anophagefferens* (Pelagophyceae). Journal of Phycology **43**: 32-42.

Quigg, A., and J. Beardall. 2003. Protein turnover in relation to maintenance metabolism at low photon flux in two marine microalgae. Plant Cell and Environment **26**: 693-703.

R Core Team. 2018. R: A language and environment for statistical computing. R Foundation for Statistical Computing, Vienna, Austria. URL https://www.R-project.org/.

Reeves, S., A. McMinn, and A. Martin. 2011. The effect of prolonged darkness on the growth, recovery and survival of Antarctic sea ice diatoms. Polar Biology **34**: 1019-1032.

Riedel, A., C. Michel, M. Gosselin, and B. Leblanc. 2008. Winter-spring dynamics in sea-ice carbon cycling in the coastal Arctic Ocean. Journal of Marine Systems **74**: 918-932.

Rivkin, R. B., and M. R. Anderson. 1997. Inorganic nutrient limitation of oceanic bacterioplankton. Limnology and Oceanography **42**: 730-740.

Röttgers R. 2007. Comparison of different variable chlorophyll a fluorescence techniques to determine photosynthetic parameters of natural phytoplankton. Deep Sea Research Part I: Oceanographic Research Papers **54**: 437-451.

Sakshaug, E. 2004. Primary and secondary production in the Arctic Seas, p. 57-81. In R. Stein and R. W. MacDonald [eds.], The Organic Carbon Cycle in the Arctic Ocean. Springer.

966 Schaub, I., H. Wagner, M. Graeve, and U. Karsten. 2017. Effects of prolonged darkness
967 and temperature on the lipid metabolism in the benthic diatom *Navicula perminuta*
968 from the Arctic Adventfjorden, Svalbard. Polar Biology **40**: 1425-1439.
969 Serôdio, J., and J. Lavaud. 2011. A model for describing the light response of the
970 nonphotochemical quenching of chlorophyll fluorescence. Photosynthesis Research
971 **108**: 61-76.
972 Sicko-Goad L., E. F. Stoermer, and G. Fahnenstiel. 1986. Rejuvenation of *Melosira*
973 *granulata* (Bacillariophyceae) resting cells from the anoxic sediments of Douglas
974 lake, Michigan. I. Light microscopy and ^{14}C uptake. Journal of Phycology **22**: 22-
975 28.
976 Smayda T. J., and B. Mitchell. 1974. Dark survival of autotrophic, planktonic marine
977 diatoms. Marine Biology **25**: 195-202.
978 Veuger, B., and D. van Oevelen. 2011. Long-term pigment dynamics and diatom survival
979 in dark sediment. Limnology and Oceanography **56**: 1065-1074.
980 Wassmann, P. 2011. Arctic marine ecosystems in an era of rapid climate change. Progress
981 in Oceanography **90**: 1-17.
982 Wassmann, P., and M. Reigstad. 2011. Future Arctic Ocean seasonal ice zones and
983 implications for pelagic-benthic coupling. *Oceanography* **24**: 220-223.
984 White A. W. 1974. Growth of two facultatively heterotrophic marine centric diatoms.
985 Journal of Phycology **10**: 292-300.
986 Wood, A. M., R. Everroad, and L. Wingard. **2005.** Measuring growth rates in microalgal
987 cultures, p. 269-285. In R. A. Anderson [eds.], Algal culturing techniques. Elsevier
988 Academic Press.
989 Wu, H. Y., A. M. Cockshutt, A. McCarthy, and D. A. Campbell. 2011. Distinctive
990 photosystem II photoinactivation and protein dynamics in marine diatoms. Plant
991 Physiology **156**: 2184-2195.
992 Wulff, A., M. Y. Roleda, K. Zacher, and C. Wiencke. 2008. Exposure to sudden light burst
993 after prolonged darkness - a case study on benthic diatoms in Antarctica. Diatom
994 Research **23**: 519-532.
995 Zapata, M., F. Rodrìguez, and J. L. Garrido. 2000. Separation of chlorophylls and
996 carotenoids from marine phytoplankton: a new HPLC method using a reversed
997 phase C8 column and pyridine-containing mobile phases. Marine Ecology Progress
998 Series **195**: 29-45.
999 Zhang, Q., R. Gradinger, and M. Spindler. 1998. Dark survival of marine microalgae in the
1000 high Arctic (Greenland Sea). Polarforschung **65**: 111-116
1001
1002

Figure legends

Figure 1. Timeline of the sampling strategy

Before dark transition, cultures were grown under stable light conditions for 52 days. Cultures were then transferred to complete darkness (grey arrow) at 'day 0' (t0 in the following figures). The vertical lines show the times of sampling, and the dashed lines show transfer of a fraction of the replicate cultures to Light return 1 after 1.5 months (48 days) and Light return 2 after 3 months (90 days) of dark incubation. Upon light return, dark acclimated subsamples were transferred to the same light conditions as before darkness.

Figure 2. Cells and reserves

a) Biovolume (μm^3, red) and Cell number per ml (blue); **b)** Cell volume (μm^3, red) and lipid droplets cell quota (RFU, blue); **c)** μg carbon (red) and μg nitrogen per cell (blue) of *Fragilariopsis cylindrus* cultures kept in the dark at 0°C for up to 3 months and then re-exposed to continuous light of 30 μmol photons m^{-2} s^{-1} after 1.5 months or 3 months of darkness for the light return experiments 1 and 2, respectively. Values from the light return experiments are shown enlarged in Fig. S6. Each point is the mean of the three cultures with the standard deviation as the error bar, except for the carbon points after the first month of darkness from which a divergent culture replicate was discarded (red dots) from the mean and standard deviation calculations.

Figure 3. Photosynthetic and photoprotective pigments

a) μg Chlorophyll *a* (Chl*a*, red) and Fucoxanthin per cell (Fuco, blue); **b)** μg Diadinoxanthin (DD, red) and Diatoxanthin per cell (DT, blue); **c)** the effective absorption cross-section for PSII photochemistry (σ_{PSII}, $Å^2$ $quanta^{-1}$, red) and photosynthetic / photoprotective pigments (Chl*a* + Chl*c* + Fuco / DD + DT, blue) of *Fragilariopsis cylindrus* cultures kept in the dark at 0°C for up to 3 months and then re-exposed to continuous light of 30 μmol photons m^{-2} s^{-1} after 1.5 months or 3 months of darkness for the light return experiments 1 and 2, respectively. Values from the light return experiments are

shown enlarged in Fig. S8. Each point is the mean of the three cultures with the standard deviation as the error bar.

Figure 4. Photosynthethic proteins and photosynthesis parameters

a) μg PsbA (PSII protein D1, red) and μg RbcL per cell (RuBisCO large subunit, blue); **b)** α (initial slope of carbon fixation, [μg C cell^{-1} h^{-1} (μmol photons m^{-2} s^{-1})$^{-1}$], red) and Φ_M (maximum quantum yield of PSII, dimensionless, blue); **c)** P_{max} (maximum carbon fixation rate, μg C cell^{-1} h^{-1}, red) and rETRmax (maximum relative electron transport rate, dimensionless, blue) of *Fragilariopsis cylindrus* cultures kept in the dark at 0°C for up to 3 months and then re-exposed to continuous light of 30 μmol photons m^{-2} s^{-1} after 1.5 months or 3 months of darkness for the light return experiments 1 and 2, respectively. Values from the light return experiments are shown enlarged in Fig. S9. Each point is the mean of the three cultures with the standard deviation as the error bar, except for the PsbA Light return 1 points from which a culture replicate was discarded (red dots) of the mean and standard deviation calculations. Note that other samples for PsbA (after 2 months of darkness and during Light return 2, red dots) and RbcL (after 2 months of darkness, during Light return 1 until day 1 and during Light return 2, blue dots) are to be treated with caution as most of them were detectable but did not fall into a quantifiable range.

Figure 5. ^{14}C incubation curves

a) Carbon fixation *vs*. irradiance curves (μg C cell^{-1} h^{-1}) of *Fragilariopsis cylindrus* cultures kept in the dark at 0°C for up to 3 months and then exposed to continuous light of 30 μmol photons m^{-2} s^{-1} after **b)** 1.5 months (Light return 1) or **c)** 3 months of darkness (Light return 2). Each curve is fitted on data points pooled from three cultures for each sampling time.

Figure 6. Photoprotective capacity

a) NPQ developed at 30 μmol photons m^{-2}s^{-1} (NPQ30, dimensionless, red) and De-epoxidation state of Diadinoxanthin (DES, blue) of *Fragilariopsis cylindrus* cultures kept in the dark at 0°C for up to 3 months and then re-exposed to continuous light of 30 μmol

1062 photons m^{-2} s^{-1} after 1.5 months (Light return 1) or **b)** 3 months of darkness (Light return 2).
1063 Each point is the mean of the three cultures with the standard deviation as the error bar.
1064
1065 **Figure 7. Scheme of the acclimation processes in *Fragilariopsis cylindrus* to prolonged**
1066 **darkness and the return of light**
1067 Acclimation processes are summarized by their levels, shown in a table with '+' and '-'
1068 signs, and as schematic representations of a *F. cylindrus* cell. Note that the 30 minutes
1069 time-points of Light return 1 (L1) and Light return 2 (L2) are not shown in the schematic
1070 representations. **Cell growth** is based on the cell number per ml and volume (μm^3)
1071 parameters. **Reserves** are based on the lipid droplets cell quota (RFU) and the carbon and
1072 nitrogen cell quotas. **Photosynthetic apparatus** is based upon molecular components and
1073 photophysiology, including Photosynthetic/Photoprotective pigments (Chlorophyll *a* +
1074 Chlorophyll *c* + Fucoxanthin / Diadinoxanthin + Diatoxanthin) and PsbA (PSII protein D1)
1075 cell quotas and with rETRmax (maximum relative electron transport rate), NPQ (non-
1076 photochemical quenching) and P_{max} (maximum carbon fixation rate per cell). Note that
1077 rETRmax and NPQ levels are hypothesized before dark transition (day 0) as there were no
1078 measurements available for this particular sampling time. The number of photosynthetic
1079 and photoprotective pigments (green and orange oval shapes, respectively) aims to
1080 represent the measured levels per cell and their ratio to each other, rather than an exact
1081 view of the photosynthetic apparatus. Legend for levels: +++ (highest), ++ (high), + (
1082 moderately high), - (moderately low), -- (low), --- (lowest). Each level is assigned relative
1083 to the observed variation for a given parameter within the entire experiment.
1084

Supporting information legend

Table S1 Mean±SD values of sampling dark days.

Table S2 Mean±SD values of sampling Light return 1 days.

Table S3 Mean±SD values of sampling Light return 2 days.

Figure S1 Picture of *F. cylindrus* cultures grown during light acclimation.

Figure S2 Spectrum of the different light sources used during the experiments.

Figure S3 Picture of *F. cylindrus* cultures grown during the light return experiments.

Figure S4 Flow cytometry data for emitted BODIPY fluorescence

Figure S5 Φ_M determinations from PAM and FIRe fluorometers

Figure S6 Figure 2 enlarged for the light return experiments.

Figure S7 Comparison between carbon and nitrogen per cell and per ml.

Figure S8 Figure 3 enlarged for the light return experiments.

Figure S9 Figure 4 enlarged for the light return experiments.

Figure S10 $E_k{}^{14}C$ (P_{max}/α) and E_k PAM (rETRmax/α).

Figure S11 Curves of dynamic and total non-photochemical quenching.

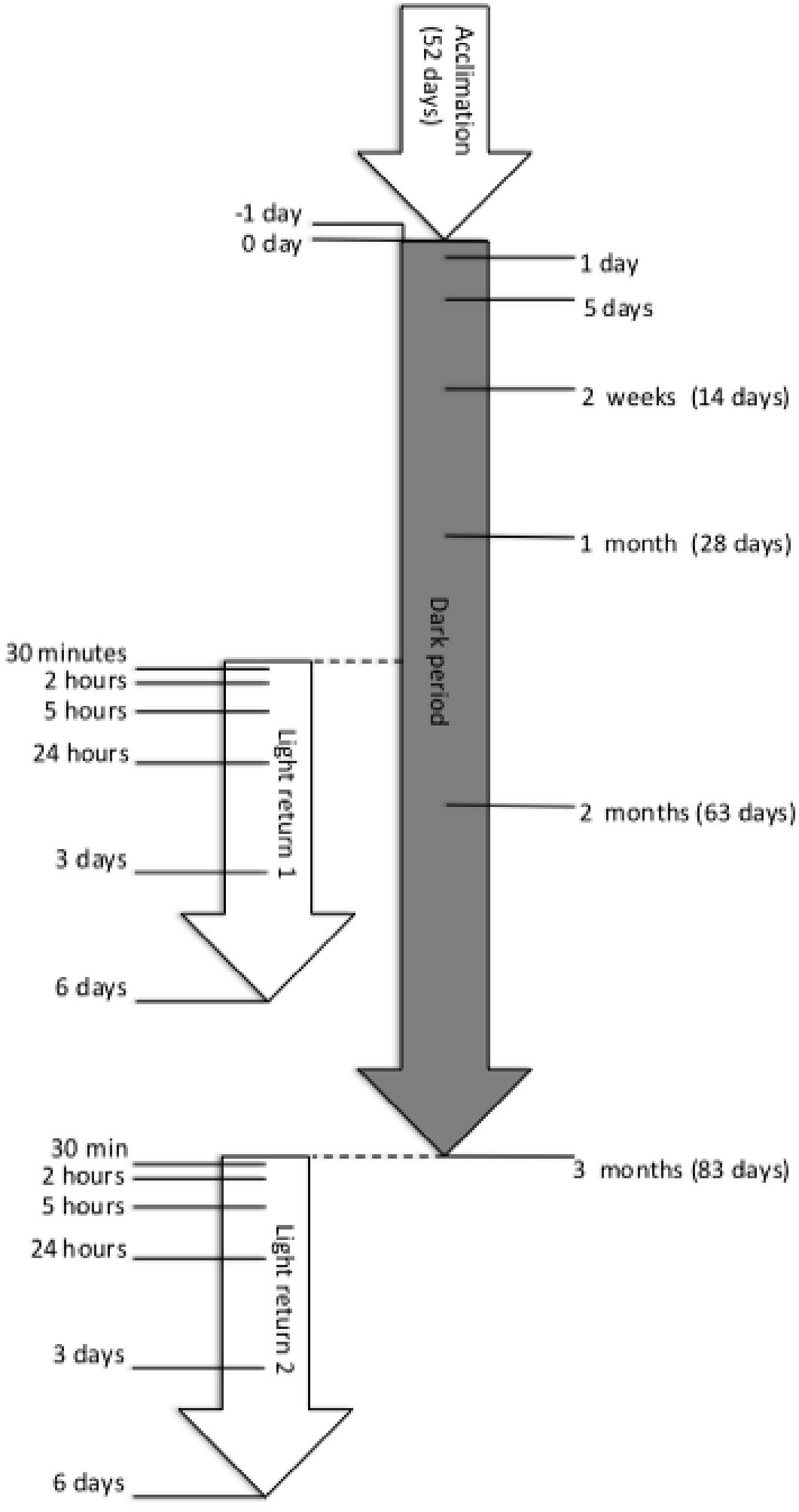
Acclimation (52 days)
-1 day
0 day
1 day
5 days
2 weeks (14 days)
1 month (28 days)
Dark period
2 months (63 days)
3 months (83 days)
30 minutes
2 hours
5 hours
24 hours
3 days
6 days
Light return 1
30 min
2 hours
5 hours
24 hours
3 days
6 days
Light return 2

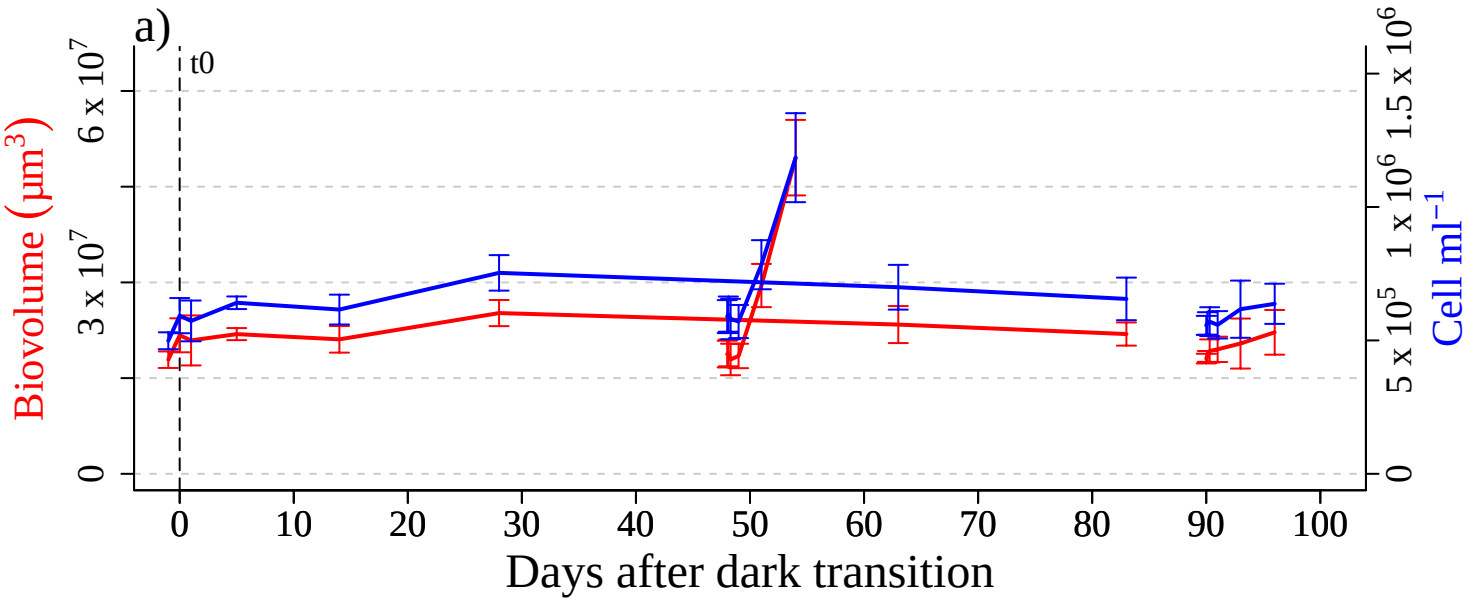
a)
t0
Biovolume (µm3)
0
3 x 10^7
6 x 10^7
Cell ml−1
0
5 x 10^5
1 x 10^6
1.5 x 10^6
0
10
20
30
40
50
60
70
80
90
100
Days after dark transition

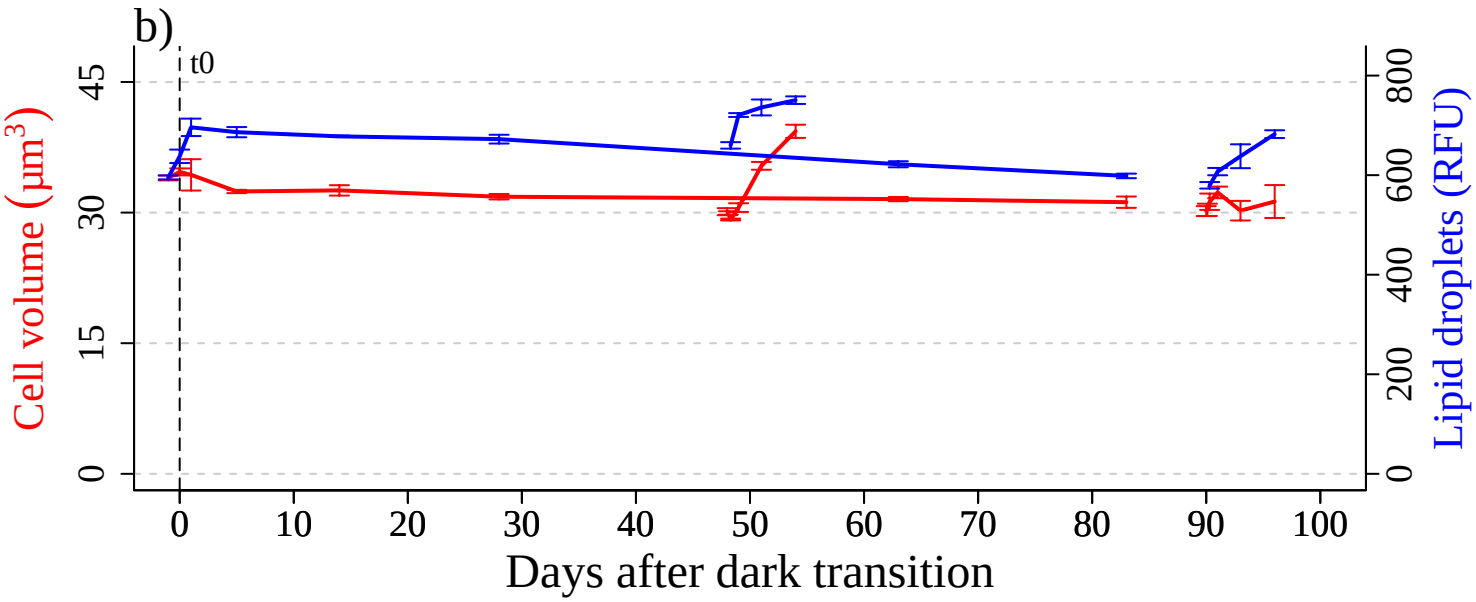
b)
t0
Cell volume (µm3)
0
15
30
45
Lipid droplets (RFU)
0
200
400
600
800
0
10
20
30
40
50
60
70
80
90
100
Days after dark transition

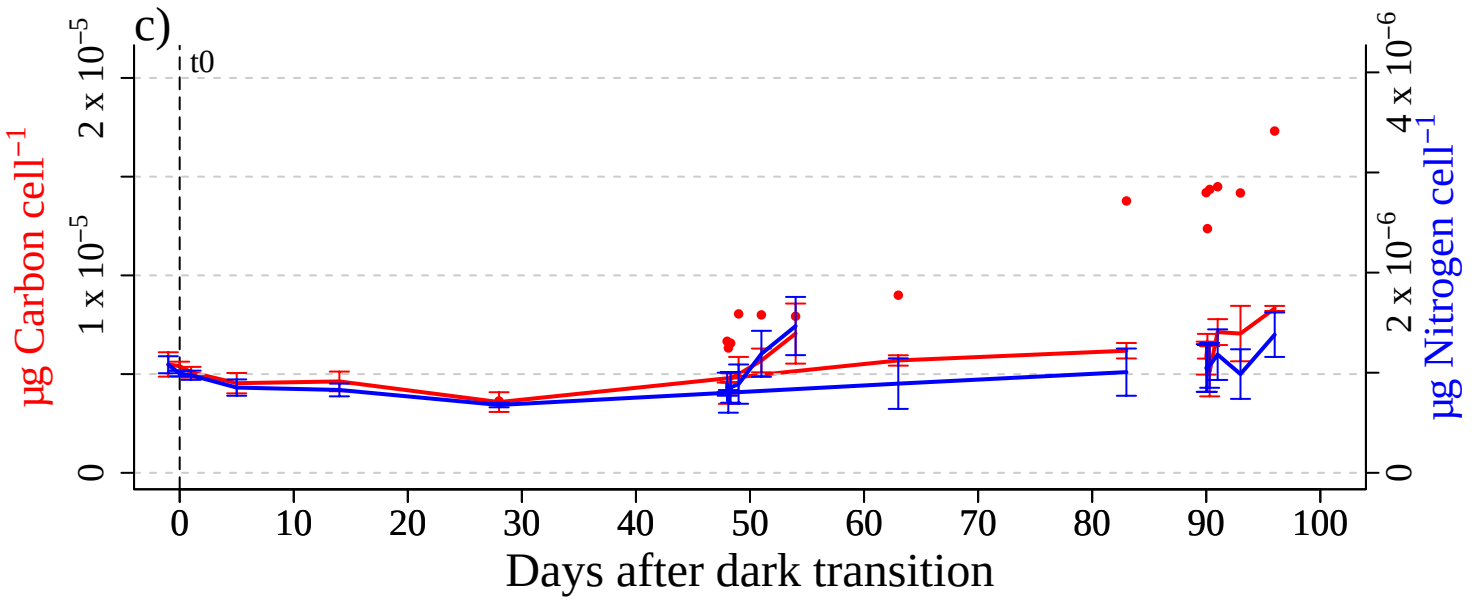
c)
t0
µg Carbon cell−1
0
1 x 10−5
2 x 10−5
µg Nitrogen cell−1
0
2 x 10−6
4 x 10−6
0
10
20
30
40
50
60
70
80
90
100
Days after dark transition

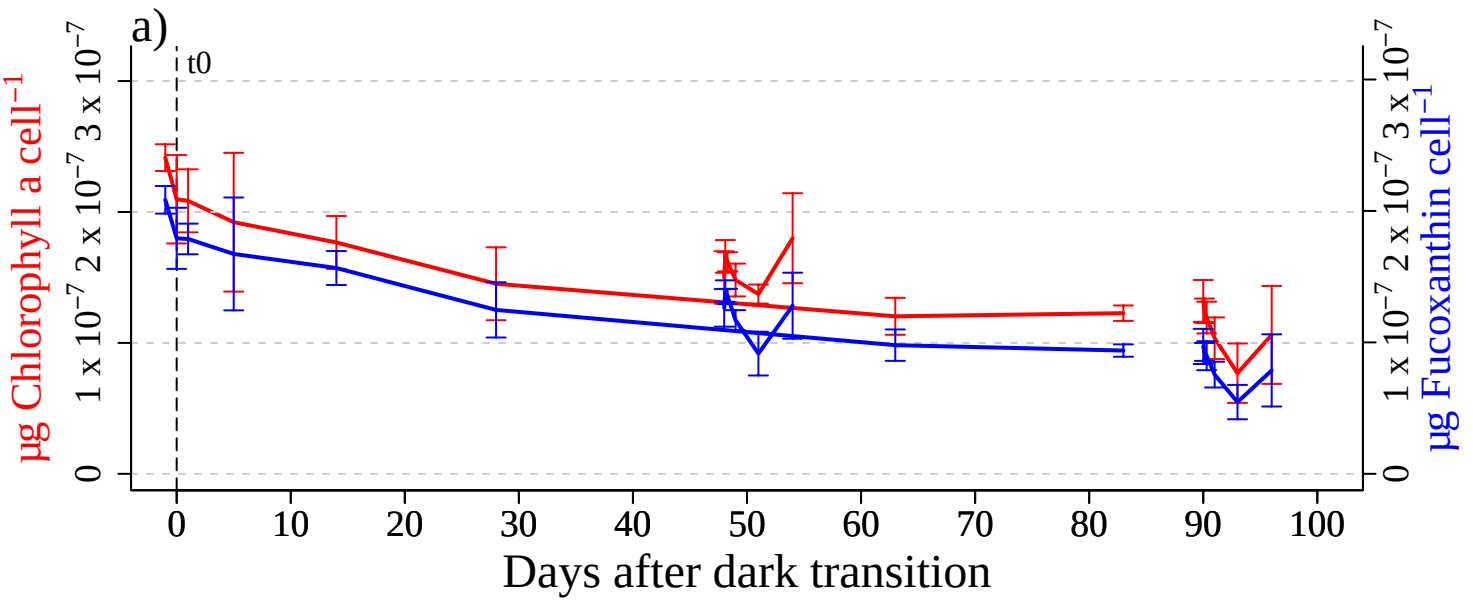
a)
t0
µg Chlorophyll a cell^{-1}
µg Fucoxanthin cell^{-1}
0
1 x 10^{-7}
2 x 10^{-7}
3 x 10^{-7}
0 10 20 30 40 50 60 70 80 90 100
Days after dark transition

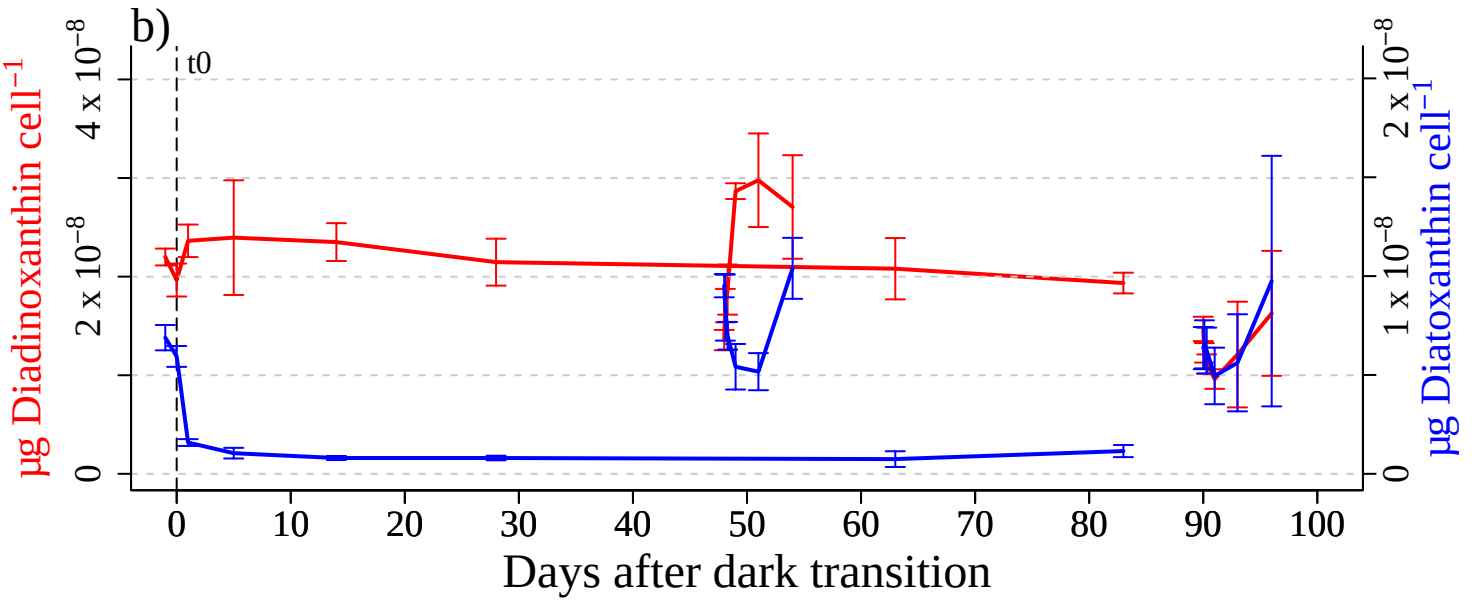
b)
t0
µg Diadinoxanthin cell^{-1}
µg Diatoxanthin cell^{-1}
0
2 x 10^{-8}
4 x 10^{-8}
1 x 10^{-8}
2 x 10^{-8}
0 10 20 30 40 50 60 70 80 90 100
Days after dark transition

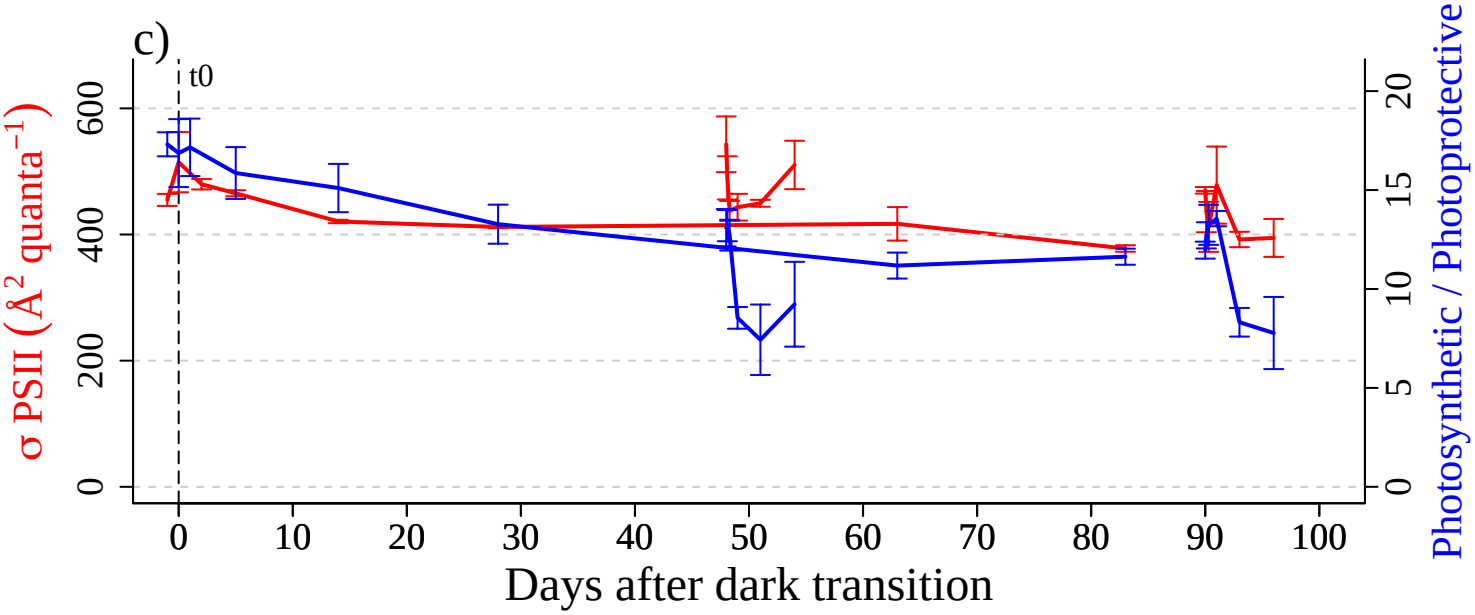
c)
t0
σ PSII (Å^2 quanta^{-1})
Photosynthetic / Photoprotective
0
200
400
600
0
5
10
15
20
0 10 20 30 40 50 60 70 80 90 100
Days after dark transition

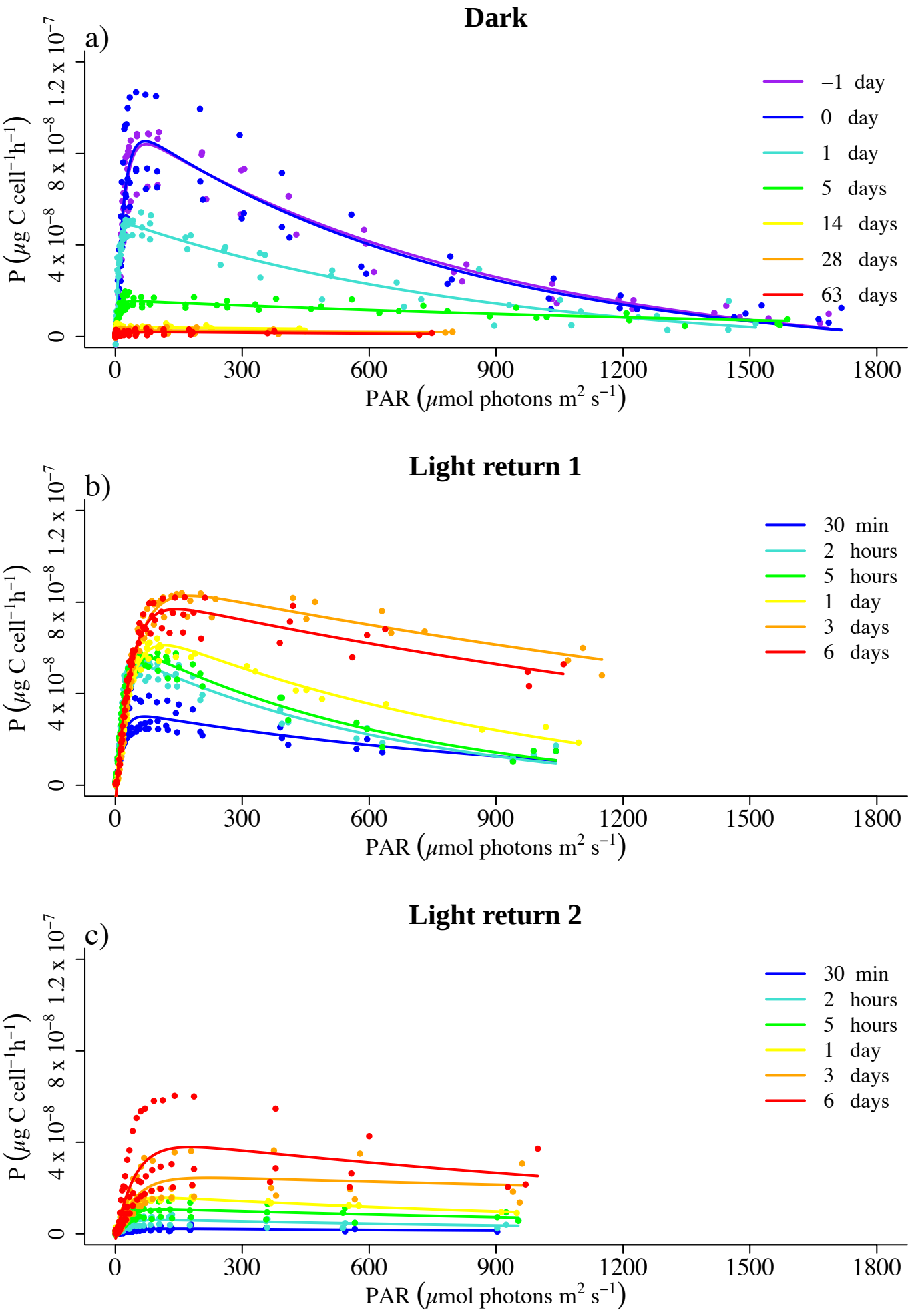
Dark
a)
P (μg C cell⁻¹h⁻¹)
0
4 x 10⁻⁸
8 x 10⁻⁸
1.2 x 10⁻⁷
0
300
600
900
1200
1500
1800
PAR (μmol photons m² s⁻¹)
−1 day
0 day
1 day
5 days
14 days
28 days
63 days
Light return 1
b)
P (μg C cell⁻¹h⁻¹)
0
4 x 10⁻⁸
8 x 10⁻⁸
1.2 x 10⁻⁷
0
300
600
900
1200
1500
1800
PAR (μmol photons m² s⁻¹)
30 min
2 hours
5 hours
1 day
3 days
6 days
Light return 2
c)
P (μg C cell⁻¹h⁻¹)
0
4 x 10⁻⁸
8 x 10⁻⁸
1.2 x 10⁻⁷
0
300
600
900
1200
1500
1800
PAR (μmol photons m² s⁻¹)
30 min
2 hours
5 hours
1 day
3 days
6 days

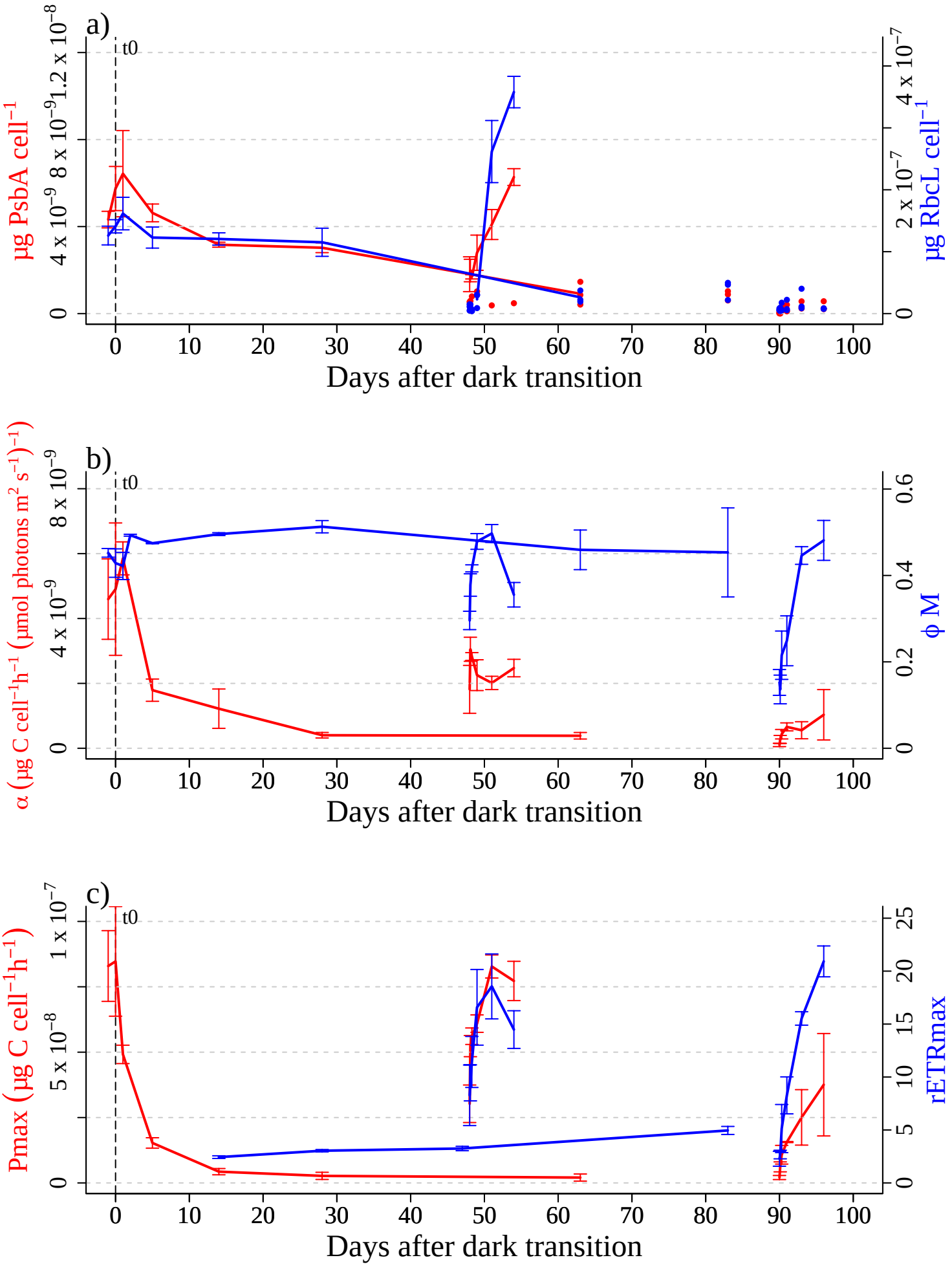
a)
t0
µg PsbA cell⁻¹
µg RbcL cell⁻¹
0
4 x 10⁻⁹
8 x 10⁻⁹
1.2 x 10⁻⁸
2 x 10⁻⁷
4 x 10⁻⁷
0 10 20 30 40 50 60 70 80 90 100
Days after dark transition
b)
t0
α (µg C cell⁻¹h⁻¹ (µmol photons m² s⁻¹)⁻¹)
ϕ M
0
4 x 10⁻⁹
8 x 10⁻⁹
0.2
0.4
0.6
0 10 20 30 40 50 60 70 80 90 100
Days after dark transition
c)
t0
Pmax (µg C cell⁻¹h⁻¹)
rETRmax
0
5 x 10⁻⁸
1 x 10⁻⁷
5
10
15
20
25
0 10 20 30 40 50 60 70 80 90 100
Days after dark transition

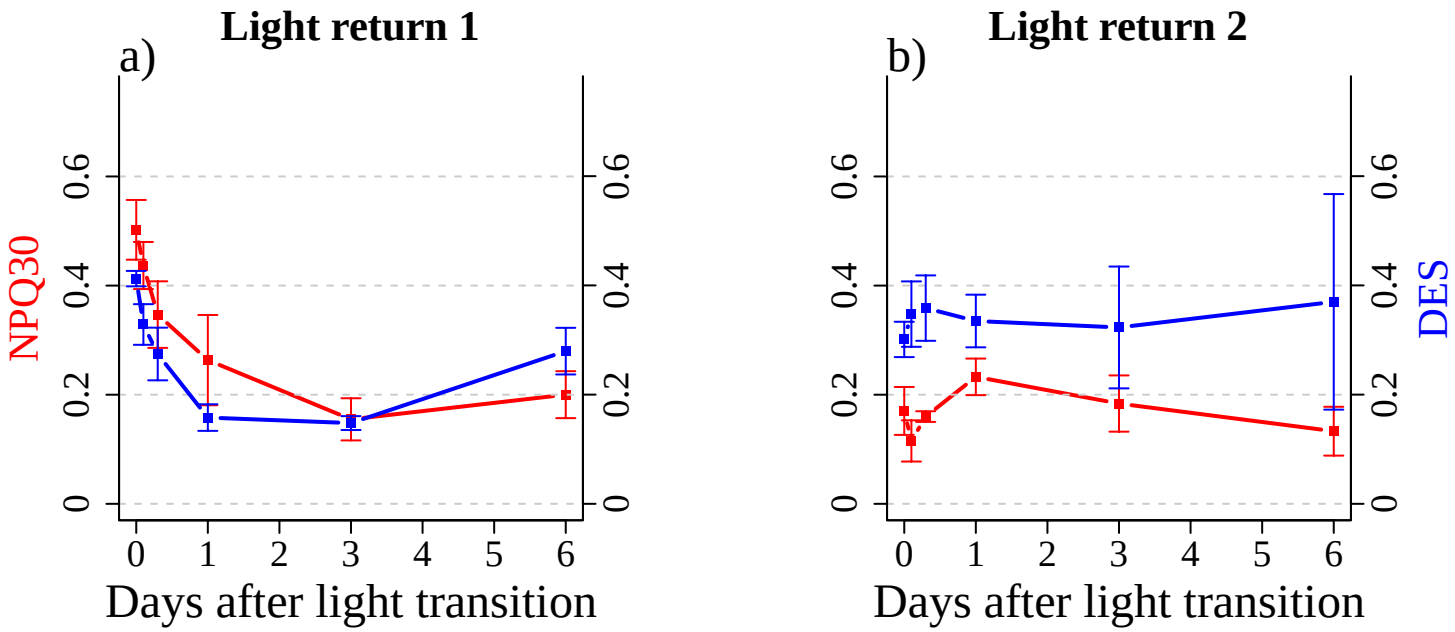
Light return 1
a)
NPQ30
0
0.2
0.4
0.6
0
1
2
3
4
5
6
Days after light transition
Light return 2
b)
DES
0
0.2
0.4
0.6
0
1
2
3
4
5
6
Days after light transition

Time	Cell growth	Reserves	Photosynthetic apparatus				
			Molecular components		Photophysiology		
			Photosynthetic/Photoprotective pigments	PsbA	rETRmax	NPQ	Pmax
D: 0 months	+	++	+++	+++	+++	+	+++
D: 1 month	++	++	++	+	- - -	+++	- - -
D: 3 months	+	+	+	- - -	- - -	+++	- - -
L1: 30 min	+	++	++	-	+	+++	+
L1: 1 day	+	+++	-	+	+++	++	+++
L1: 6 days	+++	+++	+	+++	+++	+	+++
L2: 30 min	+	+	+	- - -	+	+	-
L2: 1 day	+	+	+	- -	++	+++	+
L2: 6 days	+	++	-	- -	+++	++	++